IEEE Access
Multidisciplinary ⋮ Rapid Review ⋮ Open Access Journal

Received 26 May 2023, accepted 18 June 2023, date of publication 22 June 2023, date of current version 3 July 2023.

Digital Object Identifier 10.1109/ACCESS.2023.3288573

RESEARCH ARTICLE

A Two-Stage Method for Short-Wave Target Localization Using DOA and TDOA Measurements

LINQIANG JIANG, TAO TANG, ZHIDONG WU, PAIHANG ZHAO, AND ZIQIANG ZHANG
Institute of Information Engineering, PLA Strategic Support Force Information Engineering University, Zhengzhou 450001, China
Corresponding author: Tao Tang (13703820621@163.com)

ABSTRACT The ionosphere can make the short-wave source localization problem further non-linear, leading to a complicated solution process. This paper proposed a coordinated positioning algorithm based on the ionospheric virtual height (IVH) model to jointly estimate the target position and ionosphere reflection height using direction of arrival (DOA) and time difference of arrival (TDOA) measurements. The method is divided into two stages, the first stage is DOA localization and the second stage is TDOA localization. For the difficulty of establishing the pseudo-linear equation of elevation angle in the first stage, this paper proposed solving quadratic equations to establish the pseudo-linear equation. Moreover, since the TDOA pseudo-linear equations require the target position, the TDOA pseudo-linear equations can be established based on the estimates of DOA stage, which can lead to cooperative localization. Based on the pseudo-linear equations, the short-wave source localization problem is modeled as an optimization problem with double quadratic equation constraints. This paper proposed to solve the optimization problem combining the differentiable exact penalty method. The proposed method has a larger convergence region and requires fewer iterations to converge than the Lagrange method. Theoretical analysis shows that the localization performance of the proposed method can reach the Cramér-Rao lower bound (CRLB) and has higher accuracy than single parameter localization. Finally, the validity of theoretical analysis and the differentiable exact penalty method is verified by simulations.

INDEX TERMS Differentiable exact penalty method, direction of arrival, time difference of arrival, short-wave.

I. INTRODUCTION

Because of long-distance transmission and simple equipment setup, short-wave communication is an important method in military communications. And short-wave source localization has important applications in military and civilian [1], [2], [3], [4]. During the propagation of skywaves, short-wave source localization is very difficult owing to the time-varying nature of the ionosphere [1], [5], [6]. Therefore, studying the positioning algorithm of short-wave source is important in passive location. To narrow the research scope, this paper mainly studies the coordinated positioning method using direction of arrival (DOA) and time difference of arrival (TDOA) measurements.

DOA positioning is a common method and many algorithms have been proposed in recent years. Chen et al. [7] proposed a semidefinite relaxation method for unified near-field and far-field localization by DOA. The algorithm utilizes the modified polar to denote the source thereby alleviating the effect of numerical problem. Based on the pseudo-linear estimator, Nguyen et al. [8] proposed a Bayesian pseudo-linear estimator based on the Bayesian linear least mean square criterion. Badriasl et al. [9] proposed a new closed-form method for the three-dimensional (3D) target tracking problem using azimuth and elevation. And Badriasl et al. analyzed the localization bias. Pang et al. [10] proposed new pseudo-linear estimation algorithms for target motion analysis in the presence of sensor location errors. However, algorithms mentioned above are proposed for line-of-sight scenario, so pseudo-linear equations can be obtained directly from azimuth and elevation measurement models without

The associate editor coordinating the review of this manuscript and approving it for publication was Jiafeng Xie.

This work is licensed under a Creative Commons Attribution-NonCommercial-NoDerivatives 4.0 License.
For more information, see https://creativecommons.org/licenses/by-nc-nd/4.0/

introducing auxiliary variables. In the short-wave scenario, the azimuth is mainly used for positioning while the elevation angle is not included. In addition, the elevation measurement model changes nonlinearly in the short-wave scenario compared to the line-of-sight scenario. Therefore, above algorithms are not available for short-wave scenario.

TDOA positioning is also a common technology for short-wave source localization. Compared with DOA based localization, TDOA positioning needs to know the length of propagation path. Therefore, we need to build the corresponding ionosphere model. At present, Quasi-Parabolic (QP) model [11], [12] is commonly used for TDOA-based localization in short-wave scenario. QP model provides analytic expressions of oblique propagation and we can obtain propagation time of different path. Wang et al. [3] proposed a method using TDOAs of multiple distant receivers, which has three stages. The first two stages are used to find the optimal flying angle, and the third stage is used to get estimate of the target by Quasi-Newton method. Huang et al. [13] proposed the projected gradient-type algorithm under QP model. However, QP model involves many ionosphere parameters, which are difficult to obtain in practical applications. The ionospheric virtual height (IVH) model [1], [2], [14] only needs the reflection height to obtain the path length, which can effectively simplify the positioning problem. Wang et al. [15] investigates a new method for high-frequency geolocation without ionosphere information based on DOA and TDOA of multipaths. Zhang T et al. [16] proposed the grid-based method which is divided into test stage and search stage. However, TDOA localization based on IVH model requires target location information [17] to establish pseudo-linear equation, so it is difficult to localization using TDOA only.

The reflection height can be measured by techniques such as backscatter inversion [18], [19], [20]. Reflection height errors can cause significant performance degradation for the algorithm. Like the processing for sensor location errors [21], [22], the reflection height is considered as unknown parameter. And we jointly estimate the target location and reflection height.

Based on the IVH model, short-wave DOA and TDOA positioning can be modelled as optimization problem with double quadratic equation constraints. The first constraint is the relationship between the target and auxiliary variables which is essentially different from the constraints in [23] and [24], so we can hardly give the optimal solution in closed form. The second constraint is the geographic constraint of the target which is located at the Earth surface. The Lagrange multiplier algorithm [25], [26] is a very efficient method for optimization problems with multiple constraints, but it requires a good initial point to guarantee convergence [27]. Therefore, we combine the differentiable exact penalty method to expand the convergence region and reduce iterations [28].

For short-wave scenario, we proposed the coordinated localization algorithm that jointly estimates the target location and ionosphere reflection height by combining differentiable exact penalty method. The first stage is DOA localization, and the second stage is TDOA localization using DOA estimations and TDOA measurements.

TABLE 1. Symbols and notations.

Symbol	Explanation
$diag(\mathbf{g})$	Diagonal matrix formed by vectors
$blkdiag(\mathbf{g})$	Block-diagonal matrix composed of matrices or vectors
$(\mathbf{g})^{\mathrm{T}}$	Transpose
$\mathrm{E}(\mathbf{g})$	Mathematic expectation
$\|\mathbf{g}\|_2$	Euclidean norm
$\mathbf{¡}^{n\times m}$	$n\times m$ real matrices
$<\mathbf{g}>_i$	The ith element of the vector
$\Pi(\mathbf{g})$	Orthogonal projection matrix onto range $[\mathbf{g}]$
$\Pi^{\perp}(\mathbf{g})$	Orthogonal projection matrix onto the orthogonal subspace of range $[\mathbf{g}]$
$\mathbf{I}_M$	Identity matrix
$\mathbf{0}_{n\times m}$	Zero matrix

The main contributions of this paper are as follows:

(1) We proposed a two-stage algorithm to jointly estimate target position and ionosphere reflection height. Results of the first stage (DOA stage) can be used to establish the optimization problem of the second stage (TDOA stage) which is difficult to obtain only using TDOA measurements. And the accuracy of the second stage can achieve the Cramér–Rao lower bound (CRLB) of hybrid localization.

(2) Owing to the highly nonlinear character of the elevation measurement model, the pseudo-linear equations are difficult to establish. We proposed to establish the pseudo-linear equation by solving the quadratic equation.

(3) The exact penalty methods have satisfactory convergence properties. In order to enlarge the convergence region of Lagrange methods, we combine Lagrange methods with the exact penalty methods.

(4) We derive a closed-form expression for the mean square error (MSE) of the localization of the proposed algorithm in a first-order perturbation analysis. Theoretical analyses and simulation results show that the proposed algorithm can achieve the CRLB in two stages with moderate measurement noise and reflection height errors.

The remainder of this paper is scheduled as follows: Section II shows measurement models of DOA and TDOA; Section III establishes pseudo-linear equations of DOA and TDOA; Section IV gives the Cramér–Rao lower bound derivation; Section V is the proposed algorithm and performance analysis; Section VI presents the results of simulation; Section VII is the conclusion. Symbols used in this paper are described in TABLE 1.

II. MEASUREMENT MODEL

Consider a scenario of M stations on the Earth surface to locate a stationary target. The longitude and latitude of the ith station are $\omega_{i,1}$ and $\omega_{i,2}$, respectively. $\omega_{\mathbf{u},1}$ and $\omega_{\mathbf{u},2}$ are

the longitude and latitude of the target respectively. Based on (1), position vectors of the target and the ith station are given by $\mathbf{u}^o = [\mathbf{u}_x^o, \mathbf{u}_y^o, \mathbf{u}_z^o]^{\mathrm{T}}$ and $\mathbf{s}_i^o = [\mathbf{s}_{ix}^o, \mathbf{s}_{iy}^o, \mathbf{s}_{iz}^o]^{\mathrm{T}}$ in geocentric coordinates, respectively.

$$\begin{bmatrix} x \\ y \\ z \end{bmatrix} = \begin{bmatrix} \cos(\omega_2)\cos(\omega_1) \\ \cos(\omega_2)\sin(\omega_1) \\ (1-e^2)\sin(\omega_2) \end{bmatrix} \frac{R_e}{\sqrt{1-(e\sin(\omega_2))^2}}, \quad (1)$$

where ω_1 and ω_2 represent longitude and latitude, respectively. R_e is the equatorial radius and e is the eccentricity.

In FIGURE 1, θ_i^o and φ_i^o are the true azimuth and elevation of the ith station, respectively. h_i^o is the reflection height and R_o is the earth radius. 'True path' represents the true path of the signal propagation in the ionosphere. 'Virtual signal path' represents the equivalent path based on the IVH model and '$\boldsymbol{A}$' is the corresponding reflection point. '$\boldsymbol{B}$' represents the point where the station located. '$\boldsymbol{C}$' represents the center of Earth. The measurement model of h_i^o can be given as $\mathbf{h} = \mathbf{h}^o + \mathbf{n_h}$, where $\mathbf{h}^o = [h_1^o, h_2^o, \ldots, h_3^o]^{\mathrm{T}}$ and $\mathbf{n_h} = [\Delta h_1^o, \Delta h_2^o, \ldots, \Delta h_M^o]^{\mathrm{T}}$ is the noise vector with covariance matrix $\mathbf{Q_h}$.

As the target is assumed on the Earth surface, the target location satisfies

$$\mathbf{u}^{o\mathrm{T}}\mathbf{\Lambda}_1\mathbf{u}^o - R_e^2 = 0. \quad (2)$$

where $\mathbf{\Lambda}_1 = diag(1, 1, 1/(1-e^2))$. Since the third dimension of $\mathbf{u}^o$ can be derived by (2), the unknown parameters of $\mathbf{u}^o$ are reduced from three to two.

A. DOA MEASUREMENT MODEL

Based on FIGURE 1, θ_i^o can be given as

$$\theta_i^o = \arctan((\mathbf{b}_{i,1}^{\mathrm{T}}(\mathbf{u}^o - \mathbf{s}_i^o))/(\mathbf{b}_{i,2}^{\mathrm{T}}(\mathbf{u}^o - \mathbf{s}_i^o))), 1 \le i \le M.$$
$$\mathbf{b}_{i,2}^{\mathrm{T}} = [-\cos(\omega_{i,1})\sin(\omega_{i,2}), -\sin(\omega_{i,1})\sin(\omega_{i,2}), \cos(\omega_{i,2})] \quad (3)$$

and

$\mathbf{b}_{i,1}^{\mathrm{T}} = [-\sin(\omega_{i,1}), \cos(\omega_{i,1}), 0]$ are vectors that relate the local level coordinate system of the ith station to the geocentric coordinates. The collection of azimuth measurements forms $\boldsymbol{\theta} = [\theta_1, \theta_2, \ldots, \theta_M]^{\mathrm{T}} = \boldsymbol{\theta}^o + \mathbf{n}_{\boldsymbol{\theta}}$, where $\boldsymbol{\theta}^o = [\theta_1^o, \theta_2^o, \ldots, \theta_M^o]^{\mathrm{T}}$ and the noise vector $\mathbf{n}_{\boldsymbol{\theta}} = [\Delta\theta_1^o, \Delta\theta_2^o, \ldots, \Delta\theta_M^o]^{\mathrm{T}}$ with covariance matrix $\mathbf{Q}_{\boldsymbol{\theta}}$.

Using the law of sines in ΔABC gives

$$\begin{aligned}(h_i^o + R_o)/\sin(\pi/2 + \varphi_i^o) \\ = R_o/\sin(\pi - (\pi/2 + \varphi_i^o + \beta_i))\end{aligned} \quad (4)$$

where $\beta_i = \arcsin(||\mathbf{u}^o - \mathbf{s}_i^o||_2/2R_o)$. We can rearrange (4) as $(h_i^o + R_o)\cos(\varphi_i^o + \beta_i) = R_o\cos(\varphi_i^o)$. And dividing both sides of the equation by $\cos(\varphi_i^o)$ gives

$$(h_i^o + R_o)(\cos(\beta_i) - \tan(\varphi_i^o)\sin(\beta_i)) = R_o. \quad (5)$$

The φ_i^o can be expressed as

$$\varphi_i^o = \arctan(((R_o + h_i^o)\cos(\beta_i) - R_o)/((R_o + h_i^o)\sin(\beta_i))). \quad (6)$$

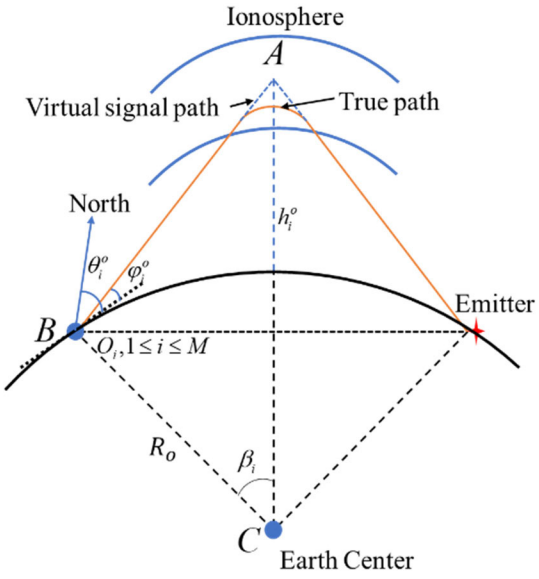

FIGURE 1. Stations receive signals which are reflected by the ionosphere from the emitter.

The measurement vector of elevation is denoted by $\boldsymbol{\varphi} = [\varphi_1, \varphi_2, \ldots, \varphi_M]^{\mathrm{T}} = \boldsymbol{\varphi}^o + \mathbf{n}_{\boldsymbol{\varphi}}$. Where $\boldsymbol{\varphi}_i = [\varphi_1^o, \varphi_2^o, \ldots, \varphi_M^o]^{\mathrm{T}}$ and $\mathbf{n}_{\boldsymbol{\varphi}} = [\Delta\varphi_1^o, \Delta\varphi_2^o, \ldots, \Delta\varphi_M^o]^{\mathrm{T}}$ is vector of zero-mean Gaussian measurement noises with covariance matrix $\mathbf{Q}_{\boldsymbol{\varphi}}$.

We collect measurements of azimuth and elevation to form the $2M \times 1$ DOA measurements vector $\mathbf{z}_1 = [\boldsymbol{\theta}^{\mathrm{T}}, \boldsymbol{\varphi}^{\mathrm{T}}]^{\mathrm{T}} = \mathbf{z}_1^o + \mathbf{n}_1$, where $\mathbf{z}_1^o = [\boldsymbol{\theta}^{o\mathrm{T}}, \boldsymbol{\varphi}^{o\mathrm{T}}]^{\mathrm{T}}$ and $\mathbf{n}_1 = [\mathbf{n}_{\boldsymbol{\theta}}^{\mathrm{T}}, \mathbf{n}_{\varphi}^{\mathrm{T}}]^{\mathrm{T}}$. Since $\mathbf{n}_{\boldsymbol{\theta}}$ and $\mathbf{n}_{\boldsymbol{\varphi}}$ are assumed to be independent, the covariance matrix of $\mathbf{n}_1$ can be expressed as $\mathbf{Q}_{\mathbf{z}_1} = blkdiag(\mathbf{Q}_{\boldsymbol{\theta}}, \mathbf{Q}_{\boldsymbol{\varphi}})$.

B. TDOA MEASUREMENT MODEL

Without loss of generality, the first station is used as the reference station. The accurate TDOA given by the station pair i and 1 is

$$\tau_{i1}^o = (r_i^o/c) - (r_1^o/c), 1 \le i \le M. \quad (7)$$

$r_i^o = 2\sqrt{R_o^2(\sin(\beta_i))^2 + (R_o - R_o\cos(\beta_i) + h_i^o)^2}$ is the path length and c is the signal propagation speed. Multiplying the TDOA by c yields

$$\begin{aligned}r_{i1}^o = r_i^o - r_1^o = 2(\sqrt{a_{i,1} - a_{i,2}\cos(\beta_i)} \\ - \sqrt{a_{1,1} - a_{1,2}\cos(\beta_1)}).\end{aligned} \quad (8)$$

r_{i1}^o is the accurate range difference of arrival (RDOA), $a_{i,1} = R_o^2 + (R_o + h_i^o)^2$ and $a_{i,2} = 2R_o(R_o + h_i^o)$. We represent the RDOA measurements by the $(M-1) \times 1$ vector $\mathbf{r} = \mathbf{r}^o + \mathbf{n_r}$, where $\mathbf{r}^o = [r_{21}^o, r_{31}^o, \ldots, r_{M1}^o]^{\mathrm{T}}$ and $\mathbf{n_r} = [\Delta r_{21}^o, \Delta r_{31}^o, \ldots, \Delta r_{M1}^o]^{\mathrm{T}}$ with covariance matrix $\mathbf{Q_r}$.

Combining the DOA and TDOA measurements, we have the hybrid measurement vector $\mathbf{z} = \mathbf{z}^o + \mathbf{n}$, where $\mathbf{z}^o = [\boldsymbol{\theta}^{o\mathrm{T}}, \boldsymbol{\varphi}^{o\mathrm{T}}, \mathbf{r}^{o\mathrm{T}}]^{\mathrm{T}}$ and $\mathbf{n} = [\mathbf{n}_{\theta}^{\mathrm{T}}, \mathbf{n}_{\boldsymbol{\varphi}}^{\mathrm{T}}, \mathbf{n}_{\mathbf{r}}^{\mathrm{T}}]^{\mathrm{T}}$.

III. PSEUDO-LINEAR EQUATION

A. DOA EQUATION

We can rewrite (3) in a linear form with respect to $\mathbf{u}^o$ as

$$(\sin(\theta_i^o)\mathbf{b}_{i,2} - \cos(\theta_i^o)\mathbf{b}_{i,1})^{\mathrm{T}}\mathbf{u}^o = (\sin(\theta_i^o)\mathbf{b}_{i,2} - \cos(\theta_i^o)\mathbf{b}_{i,1})^{\mathrm{T}}\mathbf{s}_i^o. \tag{9}$$

Stacking equations (9) of all stations yields

$$\mathbf{G}_{\boldsymbol{\theta}}^o\mathbf{u}^o = \mathbf{y}_{\boldsymbol{\theta}}^o, \tag{10}$$

where

$$\mathbf{G}_{\boldsymbol{\theta}}^o = \begin{bmatrix} (\cos(\theta_1^o)\mathbf{b}_{1,1} - \sin(\theta_1^o)\mathbf{b}_{1,2})^{\mathrm{T}} \\ (\cos(\theta_1^o)\mathbf{b}_{2,1} - \sin(\theta_1^o)\mathbf{b}_{2,2})^{\mathrm{T}} \\ \vdots \\ (\cos(\theta_1^o)\mathbf{b}_{M,1} - \sin(\theta_1^o)\mathbf{b}_{M,2})^{\mathrm{T}} \end{bmatrix}$$

$$\mathbf{y}_{\boldsymbol{\theta}}^o = \begin{bmatrix} (\cos(\theta_1^o)\mathbf{b}_{1,1} - \sin(\theta_1^o)\mathbf{b}_{1,2})^{\mathrm{T}}\mathbf{s}_1^o \\ (\cos(\theta_1^o)\mathbf{b}_{2,1} - \sin(\theta_1^o)\mathbf{b}_{2,2})^{\mathrm{T}}\mathbf{s}_2^o \\ \vdots \\ (\cos(\theta_1^o)\mathbf{b}_{M,1} - \sin(\theta_1^o)\mathbf{b}_{M,2})^{\mathrm{T}}\mathbf{s}_M^o \end{bmatrix}. \tag{11}$$

Similarly, we can rewrite (6) as

$$(R_o + h_i^o)\sin(\beta_i)\sin(\varphi_i^o) = ((R_o + h_i^o)\cos(\beta_i) - R_o)\cos(\varphi_i^o), \tag{12}$$

and substituting β_i into (12) yields

$$(R_o + h_i^o)\sin(\varphi_i^o)||\mathbf{u}^o - \mathbf{s}_i^o||_2 + 2R_o^2\cos(\varphi_i^o) = (R_o + h_i^o)\cos(\varphi_i^o)\sqrt{4R_o^2 - ||\mathbf{u}^o - s_i^o||_2^2}. \tag{13}$$

Squaring both sides of (13) gives

$$c_{i,1}||\mathbf{u}^o - \mathbf{s}_i^o||_2^2 + c_{i,2}||\mathbf{u}^o - \mathbf{s}_i^o||_2 + c_{i,3} = 0, \tag{14}$$

where $c_{i,1} = (R_o + h_i^o)^2$, $c_{i,2} = 2R_o^2(R_o + h_i^o)\sin(2\varphi_i^o)$, $c_{i,3} = -4R_o^2((h_i^o)^2 + 2R_o h_i^o)$. $||\mathbf{u}^o - \mathbf{s}_i^o||_2$ is the only positive root of $c_{i,1}x^2 + c_{i,2}x + c_{i,3} = 0$. And we arrive at

$$c_{i,4} = (\sqrt{c_{i,2}^2 - 4c_{i,1}c_{i,3}} - c_{i,2})/(2c_{i,1}) = ||\mathbf{u}^o - \mathbf{s}_i^o||_2. \tag{15}$$

The proof of (15) is given in APPENDIX I. Squaring both sides of (15) yields

$$2\mathbf{s}_i^{o\mathrm{T}}\mathbf{u}^o - ||\mathbf{u}^o||_2^2 = ||\mathbf{s}_i^o||_2^2 - c_{i,4}^2,\ 1 \le i \le M. \tag{16}$$

The set of equations (16) becomes

$$\mathbf{G}_{\boldsymbol{\varphi}}^o\boldsymbol{\eta}_a^o = \mathbf{y}_{\boldsymbol{\varphi}}^o, \tag{17}$$

where

$$\mathbf{G}_{\boldsymbol{\varphi}}^o = \begin{bmatrix} 2\mathbf{s}_1^{o\mathrm{T}} & -1 \\ 2\mathbf{s}_2^{o\mathrm{T}} & -1 \\ \vdots & \vdots \\ 2\mathbf{s}_M^{o\mathrm{T}} & -1 \end{bmatrix}, \mathbf{y}_{\boldsymbol{\varphi}}^o = \begin{bmatrix} ||\mathbf{s}_1^o||_2^2 - c_{1,4}^2 \\ ||\mathbf{s}_2^o||_2^2 - c_{2,4}^2 \\ \vdots \\ ||\mathbf{s}_M^o||_2^2 - c_{M,4}^2 \end{bmatrix}, \boldsymbol{\eta}_a^o = \begin{bmatrix} \mathbf{u}^o \\ ||\mathbf{u}^o||_2^2 \end{bmatrix}. \tag{18}$$

In (18), $||\mathbf{u}^o||_2^2$ is the auxiliary variable, which is related to u^o in non-linear relationship. $\boldsymbol{\eta}_a^o$ is the unknown parameter to be determined in the source localization problem. And we can use the relationship between $||\mathbf{u}^o||_2^2$ and $\mathbf{u}^o$ to build the constrained weighted least squares (CWLS) optimization problem.

Combining (10) and (17), the DOA equation can be given as

$$\mathbf{G}_a^o\boldsymbol{\eta}_a^o = \mathbf{y}_a^o. \tag{19}$$

Here,

$$\mathbf{G}_a^o = \begin{bmatrix} \mathbf{G}_{\boldsymbol{\theta}}^o & \mathbf{0}_{M\times 1} \\ \mathbf{G}_{\boldsymbol{\varphi}}^o \end{bmatrix}, \mathbf{y}_a^o = \begin{bmatrix} \mathbf{y}_{\boldsymbol{\theta}}^o \\ \mathbf{y}_{\boldsymbol{\varphi}}^o \end{bmatrix} \tag{20}$$

B. TDOA EQUATION

We can rewrite (8) as

$$r_{j1}^o/2 + \sqrt{a_{1,1} - a_{1,2}\cos(\beta_1)} = \sqrt{a_{j,1} - a_{j,2}\cos(\beta_j)}, \tag{21}$$

where $2 \le j \le M$. Squaring both sides of (21) gives

$$a_{j,2}\cos(\beta_j) = a_{1,2}\cos(\beta_1) - r_{j1}^o\sqrt{a_{1,1} - a_{1,2}\cos(\beta_1)} + a_{j,1} - a_{1,1} - (r_{j1}^o)^2/4. \tag{22}$$

Substituting β_j into (22) yields

$$a_{j,2}\sqrt{4R_o^2 - ||\mathbf{u}^o - \mathbf{s}_j^o||_2} = 2R_o a_{j,3}, \tag{23}$$

where

$$a_{j,3} = a_{1,2}\cos(\beta_1) - r_{j1}^o\sqrt{a_{1,1} - a_{1,2}\cos(\beta_1)} + a_{j,1} - a_{1,1} - (r_{j1}^o)^2/4.$$

Squaring both sides of (23), we arrive at

$$[2a_{j,2}^2\mathbf{s}_j^{o\mathrm{T}}, -a_{j,2}^2]\begin{bmatrix} \mathbf{u}^o \\ ||\mathbf{u}^o||_2^2 \end{bmatrix} = 4R_o^2a_{j,3}^2 + a_{j,2}^2(||\mathbf{s}_j^o||_2^2 - 4R_o^2). \tag{24}$$

Stacking equations (24) yields

$$\mathbf{G}_t^o\boldsymbol{\eta}_t^o = \mathbf{y}_t^o, \tag{25}$$

where

$$\mathbf{G}_t^o = \begin{bmatrix} 2a_{2,2}^2\mathbf{s}_2^{o\mathrm{T}} & -a_{2,2}^2 \\ 2a_{3,2}^2\mathbf{s}_3^{o\mathrm{T}} & -a_{3,2}^2 \\ \vdots & \vdots \\ 2a_{3,2}^2\mathbf{s}_M^{o\mathrm{T}} & -a_{M,2}^2 \end{bmatrix}, \boldsymbol{\eta}_t^o = \begin{bmatrix} \mathbf{u}^o \\ ||\mathbf{u}^o||_2^2 \end{bmatrix}$$

$$\mathbf{y}_t^o = \begin{bmatrix} 4R_o^2a_{2,3}^2 + a_{2,2}^2(||\mathbf{s}_2^o||_2^2 - 4R_o^2) \\ 4R_o^2a_{3,3}^2 + a_{3,2}^2(||\mathbf{s}_3^o||_2^2 - 4R_o^2) \\ \vdots \\ 4R_o^2a_{M,3}^2 + a_{M,2}^2(||\mathbf{s}_M^o||_2^2 - 4R_o^2) \end{bmatrix}. \tag{26}$$

Because $a_{j,3}$ is related to the target, $\mathbf{y}_t^o$ is usually unknown without the target position. Therefore, (25) cannot be obtained using TDOA measurements solely. Combing DOA and TDOA can efficiently solve this problem [29]. We can get the estimation of the target position using DOA measurements. Therefore, (25) can be built based on the DOA stage estimation.

IV. CRLB DERIVATION

The CRLB is the lower bound on unbiased estimators [29]. The measurement vector is $\boldsymbol{\xi}_1 = [\mathbf{z}^{\mathrm{T}}, \mathbf{h}^{\mathrm{T}}]^{\mathrm{T}}$ and the unknown vector is $\boldsymbol{\xi}_2 = [\mathbf{u}^{o\mathrm{T}}, \mathbf{h}^{o\mathrm{T}}]^{\mathrm{T}}$. Therefore, the log-likelihood function of $\boldsymbol{\xi}_1$ with respect to $\boldsymbol{\xi}_2$ is expressed as

$$\begin{aligned}\ln(p\{\boldsymbol{\xi}_1|\boldsymbol{\xi}_2\}) = t &- (\mathbf{z}-\mathbf{z}^o)^{\mathrm{T}}\mathbf{Q}_{\mathbf{z}}^{-1}(\mathbf{z}-\mathbf{z}^o)/2 \\ &- (\mathbf{h}-\mathbf{h}^o)^{\mathrm{T}}\mathbf{Q}_{\mathbf{h}}^{-1}(\mathbf{h}-\mathbf{h}^o)/2, \end{aligned} \tag{27}$$

where t is the constant independent of $\boldsymbol{\xi}_2$. And the corresponding Fisher information matrix (FIM) is given as

$$\begin{aligned}\mathbf{FIM} &= \mathrm{E}\left(\frac{\partial \ln\left(p\{\boldsymbol{\xi}_1|\boldsymbol{\xi}_2\}\right)}{\partial \boldsymbol{\xi}_2}\frac{\partial \ln\left(p\{\boldsymbol{\xi}_1|\boldsymbol{\xi}_2\}\right)}{\partial \boldsymbol{\xi}_2^{\mathrm{T}}}\right) \\ &= \begin{bmatrix}\mathbf{F}_1 & \mathbf{F}_2 \\ \mathbf{F}_2^{\mathrm{T}} & \mathbf{F}_3\end{bmatrix}. \end{aligned} \tag{28}$$

Here,

$$\begin{cases}\mathbf{F}_1 = (\partial \mathbf{z}^o/\partial \mathbf{u}^{o\mathrm{T}})^{\mathrm{T}}\mathbf{Q}_{\mathbf{z}}^{-1}(\partial \mathbf{z}^o/\partial \mathbf{u}^{o\mathrm{T}}) \\ \mathbf{F}_2 = (\partial \mathbf{z}^o/\partial \mathbf{u}^{o\mathrm{T}})^{\mathrm{T}}\mathbf{Q}_{\mathbf{z}}^{-1}(\partial \mathbf{z}^o/\partial \mathbf{h}^{o\mathrm{T}}) \\ \mathbf{F}_3 = (\partial \mathbf{z}^o/\partial \mathbf{h}^{o\mathrm{T}})^{\mathrm{T}}\mathbf{Q}_{\mathbf{z}}^{-1}(\partial \mathbf{z}^o/\partial \mathbf{h}^{o\mathrm{T}}) + \mathbf{Q}_{\mathbf{h}}^{-1}. \end{cases} \tag{29}$$

The CRLB for DOA/TDOA hybrid localization without the constraint (2) can be expressed as [30]

$$\mathbf{CRLB}_1 = (\mathbf{FIM})^{-1} = \begin{bmatrix}\mathbf{X}_1 & \mathbf{X}_2 \\ \mathbf{X}_2^{\mathrm{T}} & \mathbf{X}_3\end{bmatrix}, \tag{30}$$

where $\mathbf{X}_1 \in \mathbb{R}^{3\times 3}$ is the lower bound of the target estimate and $\mathbf{X}_3 \in \mathbb{R}^{M\times M}$ is the lower bound of ionosphere reflection height estimation.

As the target is assumed on the Earth surface, the CRLB with constraint (2) for DOA/TDOA hybrid localization is given as

$$\begin{aligned}\mathbf{CRLB}_2 &= \mathbf{CRLB}_1 \\ &- \mathbf{CRLB}_1\tilde{\boldsymbol{\Lambda}}(\tilde{\boldsymbol{\Lambda}}^{\mathrm{T}}\mathbf{CRLB}_1\tilde{\boldsymbol{\Lambda}})^{-1}\tilde{\boldsymbol{\Lambda}}^{\mathrm{T}}\mathbf{CRLB}_1, \end{aligned} \tag{31}$$

where $\tilde{\boldsymbol{\Lambda}} = [\boldsymbol{\Lambda}_1\mathbf{u}^o, \mathbf{0}_{1\times M}]^{\mathrm{T}}$. Since $\mathbf{CRLB}_1$ and $\tilde{\boldsymbol{\Lambda}}$ are positive semi-definite, $(\tilde{\boldsymbol{\Lambda}}^{\mathrm{T}}\mathbf{CRLB}_1\tilde{\boldsymbol{\Lambda}})^{-1}$ is positive semi-definite. Therefore, $\mathbf{CRLB}_1\tilde{\boldsymbol{\Lambda}}(\tilde{\boldsymbol{\Lambda}}^{\mathrm{T}}\mathbf{CRLB}_1\tilde{\boldsymbol{\Lambda}})^{-1}\tilde{\boldsymbol{\Lambda}}^{\mathrm{T}}\mathbf{CRLB}_1$ is a positive semi-definite matrix. Comparison of (30) and (31) yields $\mathbf{CRLB}_1 \succeq \mathbf{CRLB}_2$, which shows that the localization performance is improved by (2). And we can rewrite (31) as

$$\mathbf{CRLB}_2 = \mathbf{T}_1(\mathbf{T}_1^{\mathrm{T}}(\mathbf{CRLB}_1)^{-1}\mathbf{T}_1)^{-1}\mathbf{T}_1^{\mathrm{T}}, \tag{32}$$

where $\mathbf{T}_1 = blkdiag\,(\boldsymbol{\Sigma}_1, \mathbf{I}_M)$ and $\Sigma_1 = \begin{bmatrix}\mathbf{I}_2 \\ -(1-e^2)\mathbf{u}_x^o/\mathbf{u}_z^o \;\; -(1-e^2)\mathbf{u}_y^o/\mathbf{u}_z^o\end{bmatrix}$. The proof of (32) is shown in APPENDIX II. Similarly, the constrained CRLB for DOA localization and TDOA localization can be expressed as

$$\mathbf{CRLB}_2^{(a)} = \mathbf{T}_1(\mathbf{T}_1^{\mathrm{T}}(\mathbf{CRLB}_1^{(a)})^{-1}\mathbf{T}_1)^{-1}\mathbf{T}_1^{\mathrm{T}}, \tag{33}$$

$$\mathbf{CRLB}_2^{(t)} = \mathbf{T}_1(\mathbf{T}_1^{\mathrm{T}}(\mathbf{CRLB}_1^{(t)})^{-1}\mathbf{T}_1)^{-1}\mathbf{T}_1^{\mathrm{T}}. \tag{34}$$

$\mathbf{CRLB}_1^{(a)}$ and $\mathbf{CRLB}_1^{(t)}$ are the CRLB without the constraint (2) for DOA localization and TDOA localization respectively. Using the definition of CRLB gives $\mathbf{CRLB}_1^{(a)} \succeq \mathbf{CRLB}_1$ and $\mathbf{CRLB}_1^{(t)} \succeq \mathbf{CRLB}_1$. Therefore, we can obtain

$$\mathbf{CRLB}_2^{(a)} \succeq \mathbf{CRLB}_2,\ \mathbf{CRLB}_2^{(t)} \succeq \mathbf{CRLB}_2. \tag{35}$$

(35) demonstrates from CRLB that DOA/TDOA hybrid localization outperforms DOA-based and TDOA-based localization.

V. PROPOSED ALGORITHM AND PERFORMANCE ANALYSIS

A. DOA STAGE

1) PROPOSED ALGORITHM OF DOA STAGE

Substituting the noisy measurements into (19) gives

$$\boldsymbol{\varepsilon}_a = \mathbf{y}_a - \mathbf{G}_a\boldsymbol{\eta}_a. \tag{36}$$

Performing first-order Taylor expansion of $\mathbf{y}_a$ and $\mathbf{G}_a$ gives

$$\begin{cases}\mathbf{y}_a \approx \mathbf{y}_a^o + \mathbf{A}_1\mathbf{n}_1 + \mathbf{A}_2\mathbf{n}_{\mathbf{h}} \\ \mathbf{G}_a \approx \mathbf{G}_a^o + \sum_{d_1=1}^{2M} < \mathbf{z}_1 >_{d_1} \mathbf{B}_{1,d_1} \\ + \sum_{d_2=1}^{M} < \mathbf{h} >_{d_2} \mathbf{B}_{1,d_2}, \end{cases} \tag{37}$$

where

$$\begin{cases}\mathbf{A}_1 = (\partial \mathbf{y}_a/\partial \mathbf{z}_1^{\mathrm{T}}),\ \mathbf{B}_{1,d_1} = (\partial \mathbf{G}_a/\partial < \mathbf{z}_1 >_{d_1}) \\ \mathbf{A}_2 = (\partial \mathbf{y}_a/\partial \mathbf{h}^{\mathrm{T}}),\ \mathbf{B}_{2,d_2} = (\partial \mathbf{G}_a/\partial < \mathbf{h} >_{d_2}). \end{cases} \tag{38}$$

Substituting (37) into (36) yields

$$\boldsymbol{\varepsilon}_a \approx \mathbf{C}_1\mathbf{n}_1 + \mathbf{C}_2\mathbf{n}_{\mathbf{h}}, \tag{39}$$

where $\mathbf{C}_1 = (\mathbf{A}_1 - [\mathbf{B}_{1,1}\boldsymbol{\eta}_a, \mathbf{B}_{1,2}\boldsymbol{\eta}_a, \ldots, \mathbf{B}_{1,2M}\boldsymbol{\eta}_a])$ and $\mathbf{C}_2 = (\mathbf{A}_2 - [\mathbf{B}_{2,1}\boldsymbol{\eta}_a, \mathbf{B}_{2,2}\boldsymbol{\eta}_a, \ldots, \mathbf{B}_{2,M}\boldsymbol{\eta}_a])$. To account for the dependency of nuisance parameters $||\mathbf{u}||_2^2$ on $\mathbf{u}$ and the relationship of (2), two constraints are introduced. The target localization problem is thus stated as follows.

$$\begin{cases}\min\limits_{\tilde{\boldsymbol{\eta}}_a} \mathrm{J}_a(\tilde{\boldsymbol{\eta}}_a) = (\tilde{\mathbf{y}}_a - \tilde{\mathbf{G}}_a\tilde{\boldsymbol{\eta}}_a)^{\mathrm{T}}\mathbf{W}_a(\tilde{\mathbf{y}}_a - \tilde{\mathbf{G}}_a\tilde{\boldsymbol{\eta}}_a) \\ \text{s.t. } \tilde{\boldsymbol{\eta}}_a^{\mathrm{T}}\tilde{\boldsymbol{\Lambda}}_1\tilde{\boldsymbol{\eta}}_a - R_e^2 = 0 \\ \tilde{\boldsymbol{\eta}}_a^{\mathrm{T}}\tilde{\boldsymbol{\Lambda}}_2\tilde{\boldsymbol{\eta}}_a + \boldsymbol{\gamma}_1^{\mathrm{T}}\tilde{\boldsymbol{\eta}}_a = 0. \end{cases} \tag{40}$$

Remark 1: The first constraint is from (2) and the second one is from the relationship between $||\mathbf{u}^o||_2^2$ and $\mathbf{u}^o$. In the solution process, the source location cannot be accurately estimated and the equation constraint is not strictly equal to zero. The optimal value $\hat{\tilde{\boldsymbol{\eta}}}_a$ not only minimizes the objective function but also the equation constraints. Therefore, two equation constraints can be used to improve the estimation performance.

Here, $\tilde{\boldsymbol{\Lambda}}_1 = blkdiag(\boldsymbol{\Lambda}_1, \mathbf{0}_{(M+1)\times(M+1)})$, $\boldsymbol{\gamma}_1 = [0, 0, 0, -1, \mathbf{0}_{1\times M}]^{\mathrm{T}}$, $\tilde{\boldsymbol{\Lambda}}_2 = blkdiag(diag(1, 1, 1, 0), \mathbf{0}_{M\times M})$ and

$$\tilde{\mathbf{y}}_a = \begin{bmatrix}\mathbf{y}_a \\ \mathbf{h}\end{bmatrix}, \tilde{\mathbf{G}}_a = \begin{bmatrix}\mathbf{G}_a & \mathbf{0}_{2M\times M} \\ \mathbf{0}_{M\times 4} & \mathbf{I}_M\end{bmatrix}, \tilde{\boldsymbol{\eta}}_a = \begin{bmatrix}\boldsymbol{\eta}_a \\ \mathbf{h}\end{bmatrix}. \tag{41}$$

$\mathbf{W}_a$ is the weighting matrix defined as

$$\mathbf{W}_a = \begin{bmatrix} \mathbf{C}_1\mathbf{Q}_{\mathbf{z}_1}\mathbf{C}_1^{\mathrm{T}} + \mathbf{C}_2\mathbf{Q}_{\mathbf{h}}\mathbf{C}_2^{\mathrm{T}} & \mathbf{C}_2\mathbf{Q}_{\mathbf{h}} \\ (\mathbf{C}_2\mathbf{Q}_{\mathbf{h}})^{\mathrm{T}} & \mathbf{Q}_{\mathbf{h}} \end{bmatrix}^{-1}. \quad (42)$$

To enlarge the convergence region of the Lagrange method, we combine the differentiable exact penalty method to solve (40). Firstly, the Lagrange function is

$$\mathrm{L}_a(\tilde{\boldsymbol{\eta}}_a, \boldsymbol{\lambda}_a) = \mathrm{J}_a(\tilde{\boldsymbol{\eta}}_a) + \boldsymbol{\lambda}_a^{\mathrm{T}}\mathbf{g}(\tilde{\boldsymbol{\eta}}_a), \quad (43)$$

where $\boldsymbol{\lambda}_a = [\lambda_1^{(a)}, \lambda_2^{(a)}]^{\mathrm{T}}$ represents the Lagrange multipliers and $\mathbf{g}(\tilde{\boldsymbol{\eta}}_a) = [g_1(\tilde{\boldsymbol{\eta}}_a), g_2(\tilde{\boldsymbol{\eta}}_a)]^{\mathrm{T}}$. Here, $g_1(\tilde{\boldsymbol{\eta}}_a) = \tilde{\boldsymbol{\eta}}_a^{\mathrm{T}}\tilde{\boldsymbol{\Lambda}}_1\tilde{\boldsymbol{\eta}}_a - R_e^2$ and $g_2(\tilde{\boldsymbol{\eta}}_a) = \tilde{\boldsymbol{\eta}}_a^{\mathrm{T}}\tilde{\boldsymbol{\Lambda}}_2\tilde{\boldsymbol{\eta}}_a + \boldsymbol{\gamma}_1^{\mathrm{T}}\tilde{\boldsymbol{\eta}}_a$. The following conditions need to be satisfied for $\tilde{\boldsymbol{\eta}}_a$ and λ_a.

$$\begin{aligned} \tilde{\mathrm{L}}_{\tilde{\boldsymbol{\eta}}_a}(\tilde{\boldsymbol{\eta}}_a, \boldsymbol{\lambda}_a) &= \partial \mathrm{L}_a(\tilde{\boldsymbol{\eta}}_a, \boldsymbol{\lambda}_a)/\partial\tilde{\boldsymbol{\eta}}_a \\ &= \tilde{\mathrm{J}}_a(\tilde{\boldsymbol{\eta}}_a) + (\tilde{\mathbf{g}}(\tilde{\boldsymbol{\eta}}_a))^{\mathrm{T}}\tilde{\boldsymbol{\lambda}} = \mathbf{0}_{(4+M)\times 1} \\ \tilde{\mathrm{L}}_{\tilde{\boldsymbol{\lambda}}_a}(\tilde{\boldsymbol{\eta}}_a) &= \partial \mathrm{L}_a(\tilde{\boldsymbol{\eta}}_a, \boldsymbol{\lambda}_a)/\partial\boldsymbol{\lambda}_a = \mathbf{g}(\tilde{\boldsymbol{\eta}}_a) = \mathbf{0}_{2\times 1}, \end{aligned} \quad (44)$$

where $\tilde{\mathbf{g}}(\tilde{\boldsymbol{\eta}}_a) = (\partial\mathbf{g}(\tilde{\boldsymbol{\eta}}_a))/(\partial\tilde{\boldsymbol{\eta}}_a^{\mathrm{T}}) = [(2\tilde{\boldsymbol{\eta}}_g^{\mathrm{T}}\tilde{\boldsymbol{\Lambda}}_1)^{\mathrm{T}}, (2\tilde{\boldsymbol{\eta}}_a^{\mathrm{T}}\tilde{\boldsymbol{\Lambda}}_2 + \boldsymbol{\gamma}_1^{\mathrm{T}})^{\mathrm{T}}]^{\mathrm{T}}$ and $\tilde{\mathrm{J}}_a(\tilde{\boldsymbol{\eta}}_a) = (\partial \mathrm{J}_a(\tilde{\boldsymbol{\eta}}_a))/(\partial\tilde{\boldsymbol{\eta}}_a) = 2\tilde{\mathbf{G}}_a\mathbf{W}_a(\tilde{\mathbf{G}}_a\tilde{\boldsymbol{\eta}}_a - \tilde{\mathbf{y}}_a)$.

Based on (43), the corresponding unconstrained optimization problem is expressed as

$$\left\{\hat{\tilde{\boldsymbol{\eta}}}_a, \hat{\boldsymbol{\lambda}}_a\right\} = \arg\min_{\tilde{\boldsymbol{\eta}}_a, \boldsymbol{\lambda}_a}(||\tilde{\mathrm{L}}_{\tilde{\boldsymbol{\eta}}_a}(\tilde{\boldsymbol{\eta}}_a, \boldsymbol{\lambda}_a)||^2/2 + ||\tilde{\mathrm{L}}_{\tilde{\boldsymbol{\lambda}}_a}(\tilde{\boldsymbol{\eta}}_a)||^2/2), \quad (45)$$

and the general penalty function. [31] is

$$\begin{aligned} \mathrm{P}_a(\tilde{\boldsymbol{\eta}}_a, \boldsymbol{\lambda}_a) = L_a(\tilde{\boldsymbol{\eta}}_a, \boldsymbol{\lambda}_a) + (\chi^{(a)} + \mu^{(a)}||\boldsymbol{\lambda}_a||^2)||\mathbf{g}(\tilde{\boldsymbol{\eta}}_a)||^2/2 \\ + ||\mathbf{M}_a(\tilde{\boldsymbol{\eta}}_a)\tilde{\mathrm{L}}_{\tilde{\boldsymbol{\eta}}_a}(\tilde{\boldsymbol{\eta}}_a, \boldsymbol{\lambda}_a)||^2/2. \end{aligned} \quad (46)$$

$\chi^{(a)} > 0$ is the penalty factor, which should be sufficiently big to make the penalty function work. And $\mu^{(a)} \geq 0$ is some fixed scalar. $\mathbf{M}_a(\tilde{\boldsymbol{\eta}}_a)$ is the continuously differentiable matrix and can be given as [30]

$$\mathbf{M}_a(\tilde{\boldsymbol{\eta}}_a) = (\tilde{\mathbf{g}}(\tilde{\boldsymbol{\eta}}_a)(\tilde{\mathbf{g}}(\tilde{\boldsymbol{\eta}}_a))^{\mathrm{T}})^{-1}\tilde{\mathbf{g}}(\tilde{\boldsymbol{\eta}}_a) \in \mathbb{R}^{2\times(4+M)}. \quad (47)$$

Based on the derivation in [31], the algorithm of DOA stage is as follows:

(1) Set $\delta^{(a)} > 0$ as the stop threshold, and choose appropriate $\chi^{(a)}$ and $\mu^{(a)}$. Initializing $\hat{\tilde{\boldsymbol{\eta}}}_a^{(0)}$, $\hat{\boldsymbol{\lambda}}_a^{(0)}$ and making $k = 0$;

(2) By applying Newton's method, $\Delta\tilde{\boldsymbol{\eta}}_a^{(k)}$ and $\Delta\boldsymbol{\lambda}_a^{(k)}$ can be given as

$$\begin{bmatrix} \Delta\tilde{\boldsymbol{\eta}}_a^{(k)} \\ \Delta\boldsymbol{\lambda}_a^{(k)} \end{bmatrix} = \begin{bmatrix} \tilde{\tilde{\mathrm{L}}}_{\tilde{\boldsymbol{\eta}}_a}(\tilde{\boldsymbol{\eta}}_a^{(k)}, \boldsymbol{\lambda}_a^{(k)}) & (\tilde{\mathbf{g}}(\tilde{\boldsymbol{\eta}}_a^{(k)}))^{\mathrm{T}} \\ \tilde{\mathbf{g}}(\tilde{\boldsymbol{\eta}}_a^{(k)}) & \mathbf{0}_{2\times 2} \end{bmatrix}^{-1} \begin{bmatrix} \tilde{\mathrm{L}}_{\tilde{\boldsymbol{\eta}}_a}(\tilde{\boldsymbol{\eta}}_a, \boldsymbol{\lambda}_a) \\ \mathbf{g}(\tilde{\boldsymbol{\eta}}_a^{(k)}) \end{bmatrix}, \quad (48)$$

where $\tilde{\tilde{\mathrm{L}}}_{\tilde{\boldsymbol{\eta}}_a}(\tilde{\boldsymbol{\eta}}_a^{(k)}, \boldsymbol{\lambda}_a^{(k)}) = 2\tilde{\mathbf{G}}_a^{\mathrm{T}}\mathbf{W}_a\tilde{\mathbf{G}}_a + 2\lambda_1^{(a)}\tilde{\boldsymbol{\Lambda}}_1 + 2\lambda_2^{(a)}\tilde{\boldsymbol{\Lambda}}_2$;

(3) Update $\hat{\tilde{\boldsymbol{\eta}}}_a^{(k+1)} = \hat{\tilde{\boldsymbol{\eta}}}_a^{(k)} + \delta_{a1}^{(k)}\Delta\hat{\tilde{\boldsymbol{\eta}}}_a^{(k)}$ and $\tilde{\boldsymbol{\lambda}}_a^{(k+1)} = \tilde{\boldsymbol{\lambda}}_a^{(k)} + \delta_{a2}^{(k)}\Delta\hat{\boldsymbol{\lambda}}_a^{(k)}$. $\delta_{a1}^{(k)}$ and $\delta_{a2}^{(k)}$ are obtained via Armijo rule based on (46);

(4) Based on $\partial \mathrm{P}_a(\tilde{\boldsymbol{\eta}}_a, \boldsymbol{\lambda}_a)/\boldsymbol{\lambda}_a = \mathbf{0}_{2\times 1}$, $\hat{\boldsymbol{\lambda}}_a^{(k+1)}$ can be expressed as

$$\begin{aligned} \hat{\boldsymbol{\lambda}}_a^{(k+1)} = -(1 + \mu^{(a)}||\mathbf{g}(\hat{\tilde{\boldsymbol{\eta}}}_a^{(k+1)})||^2)^{-1} \\ \times (\mathbf{g}(\hat{\tilde{\boldsymbol{\eta}}}_a^{(k+1)}) + \mathbf{M}_a(\hat{\tilde{\boldsymbol{\eta}}}_a^{(k+1)})\tilde{\mathbf{J}}(\hat{\tilde{\boldsymbol{\eta}}}_a^{(k+1)})); \end{aligned} \quad (49)$$

(5) Let $k = k + 1$, substituting $\hat{\tilde{\boldsymbol{\eta}}}_a^{(k)}$ and $\hat{\boldsymbol{\lambda}}_a^{(k)}$ into (46) yields $\mathrm{P}_a(\hat{\tilde{\boldsymbol{\eta}}}_a^{(k)}, \hat{\boldsymbol{\lambda}}_a^{(k)})$;

(6) If

$$\begin{aligned} (|\mathrm{P}_a(\hat{\tilde{\boldsymbol{\eta}}}_a^{(k)}, \hat{\boldsymbol{\lambda}}_a^{(k)}) \\ - \mathrm{P}_a(\hat{\tilde{\boldsymbol{\eta}}}_a^{(k-1)}, \hat{\boldsymbol{\lambda}}_a^{(k-1)})|/|\mathrm{P}_a(\hat{\tilde{\boldsymbol{\eta}}}_a^{(k-1)}, \hat{\boldsymbol{\lambda}}_a^{(k-1)})|) < \delta^{(a)}, \end{aligned}$$

the iteration process is terminated, otherwise go to (2).

In the initial stage, the weighted least squares solution of (40) can be given as $\hat{\tilde{\boldsymbol{\eta}}}_a^{(0)} = (\tilde{\mathbf{G}}_a^{\mathrm{T}}\mathbf{W}_a\tilde{G}_a)^{-1}\tilde{\mathbf{G}}_a^{\mathrm{T}}\mathbf{W}_a\tilde{\mathbf{y}}_a$ by neglecting constraints. Because $\mathbf{W}_a$ is related to the target position and thus is more difficult to obtain. We can set $\mathbf{W}_a$ as identity matrix to obtain the initial value, which does not substantially affect the final result [21], [32], [33] and can guarantee convergence of the algorithm. Therefore, $\hat{\tilde{\boldsymbol{\eta}}}_a^{(0)}$ is given as

$$\hat{\tilde{\boldsymbol{\eta}}}_a^{(0)} = (\tilde{\mathbf{G}}_a^{\mathrm{T}}\tilde{\mathbf{G}}_a)^{-1}\tilde{\mathbf{G}}_a^{\mathrm{T}}\tilde{\mathbf{y}}_a. \quad (50)$$

And $\hat{\boldsymbol{\lambda}}_a^{(0)}$ can be expressed as

$$\hat{\boldsymbol{\lambda}}_a^{(0)} = -(1 + \mu^{(a)}||\mathbf{g}(\hat{\tilde{\boldsymbol{\eta}}}_a^{(0)})||^2)^{-1}(\mathbf{g}(\hat{\tilde{\boldsymbol{\eta}}}_a^{(0)}) + \mathbf{M}_a(\hat{\tilde{\boldsymbol{\eta}}}_a^{(0)})\tilde{J}(\hat{\tilde{\boldsymbol{\eta}}}_a^{(0)})). \quad (51)$$

Main steps of the proposed algorithm in DOA stage are summarized as follows:

TABLE 2. Main steps of doa stage.

Step 1	Let $k=0$ and choose appropriate $\delta^{(a)}>0$, $\chi^{(a)}>0$, and $\mu^{(a)}\geq 0$. Calculate $\hat{\tilde{\boldsymbol{\eta}}}_a^{(0)}$ and $\hat{\boldsymbol{\lambda}}_a^{(0)}$ based on (50) and (51) respectively.
Step 2	Calculate $\Delta\tilde{\boldsymbol{\eta}}_a^{(k)}$ and $\Delta\boldsymbol{\lambda}_a^{(k)}$ based on (48).
Step 3	Update $\hat{\tilde{\boldsymbol{\eta}}}_a^{(k+1)}$ and $\tilde{\boldsymbol{\lambda}}_a^{(k+1)}$.
Step 4	Replace $\tilde{\boldsymbol{\lambda}}_a^{(k+1)}$ with $\hat{\boldsymbol{\lambda}}_a^{(k+1)}$.
Step 5	Let $k=k+1$ and calculate $\mathrm{P}_a(\hat{\tilde{\boldsymbol{\eta}}}_a^{(k)}, \hat{\boldsymbol{\lambda}}_a^{(k)})$ based on (46).
Step 6	If $(|\mathrm{P}_a(\hat{\tilde{\boldsymbol{\eta}}}_a^{(k)}, \hat{\boldsymbol{\lambda}}_a^{(k)}) - \mathrm{P}_a(\hat{\tilde{\boldsymbol{\eta}}}_a^{(k-1)}, \hat{\boldsymbol{\lambda}}_a^{(k-1)})|/|\mathrm{P}_a(\hat{\tilde{\boldsymbol{\eta}}}_a^{(k-1)}, \hat{\boldsymbol{\lambda}}_a^{(k-1)})|) < \delta^{(a)}$, then stop the iteration. If not, go to Step 2.
Step 7	Target position and ionosphere reflection height estimates are given as $\hat{\mathbf{u}}_a = \hat{\tilde{\boldsymbol{\eta}}}_a^{(k)}(1:3), \hat{\mathbf{h}}_a = \hat{\tilde{\boldsymbol{\eta}}}_a^{(k)}(4:end)$. (52)

2) PERFORMANCE ANALYSIS OF DOA STAGE

This subsection presents the performance analysis of the proposed method in DOA stage. The MSE of the proposed method is compared with $\mathbf{CRLB}_2^{(a)}$ in (33). Firstly, the estimation error is defined as $\Delta\tilde{\boldsymbol{\eta}}_a = \hat{\tilde{\boldsymbol{\eta}}}_a - \tilde{\boldsymbol{\eta}}_a^o$, where $\hat{\tilde{\boldsymbol{\eta}}}_a$ is the estimation result and $\tilde{\boldsymbol{\eta}}_a^o$ is the true value.

Performing the first-order perturbation analysis, $\Delta\tilde{\boldsymbol{\eta}}_a$ is the optimal solution of the following optimization problem:

$$\begin{cases} \min\limits_{\Delta\tilde{\boldsymbol{\eta}}_a} \left(\tilde{\mathbf{G}}_a\Delta\tilde{\boldsymbol{\eta}}_a - \begin{bmatrix}\boldsymbol{\varepsilon}_a \\ \mathbf{n_h}\end{bmatrix}\right)^{\mathrm{T}} \mathbf{W}_a \left(\tilde{\mathbf{G}}_a\Delta\tilde{\boldsymbol{\eta}}_a - \begin{bmatrix}\boldsymbol{\varepsilon}_a \\ \mathbf{n_h}\end{bmatrix}\right) \\ \text{s.t.} \quad (\Delta\tilde{\boldsymbol{\eta}}_a)^{\mathrm{T}}\tilde{\boldsymbol{\Lambda}}_1\tilde{\boldsymbol{\eta}}_a^o = 0 \\ \qquad (\Delta\tilde{\boldsymbol{\eta}}_a)^{\mathrm{T}}(2\tilde{\boldsymbol{\Lambda}}_2\tilde{\boldsymbol{\eta}}_a^o + \boldsymbol{\gamma}_1) = 0. \end{cases} \tag{53}$$

Remark 2: *The first-order perturbation analysis was used to derive the covariance matrix of the estimation error $\Delta\tilde{\boldsymbol{\eta}}_a$. And (53) is a method to derive $\Delta\tilde{\boldsymbol{\eta}}_a$ which is related to the estimation result $\hat{\tilde{\boldsymbol{\eta}}}_a$. The effect of the proposed algorithm, including penalty factor $\chi^{(a)}$ and fixed scalar $\mu^{(a)}$ is reflected in $\hat{\tilde{\boldsymbol{\eta}}}_a$. Therefore, we can analyze the performance of the proposed algorithm from $\Delta\tilde{\boldsymbol{\eta}}_a$.*

Therefore, $\Delta\tilde{\boldsymbol{\eta}}_a$ can be expressed as

$$\Delta\tilde{\boldsymbol{\eta}}_a = (\mathbf{I}_{4+M} - \boldsymbol{\Phi}_a(\boldsymbol{\Psi}_a^{\mathrm{T}}\boldsymbol{\Phi}_a\boldsymbol{\Psi}_a)^{-1}\boldsymbol{\Psi}_a^{\mathrm{T}})\boldsymbol{\Phi}_a\tilde{\mathbf{G}}_a^{\mathrm{T}}\mathbf{W}_a\left[\boldsymbol{\varepsilon}_a^{\mathrm{T}}, \mathbf{n_h}^{\mathrm{T}}\right]^{\mathrm{T}} \tag{54}$$

where $\boldsymbol{\Psi}_a = [\boldsymbol{\psi}_1^{(a)}, \boldsymbol{\psi}_2^{(a)}] = [\tilde{\boldsymbol{\Lambda}}_1\tilde{\boldsymbol{\eta}}_a^o, 2\tilde{\boldsymbol{\Lambda}}_2\tilde{\boldsymbol{\eta}}_a^o + \boldsymbol{\gamma}_1]$ and $\boldsymbol{\Phi}_a = (\tilde{\mathbf{G}}_a^{\mathrm{T}}\mathbf{W}_a\tilde{\mathbf{G}}_a)^{-1}$. APPENDIX III shows the proof of (54). Therefore, the covariance matrix of $\Delta\tilde{\boldsymbol{\eta}}_a$ is $\mathrm{cov}(\Delta\tilde{\boldsymbol{\eta}}_a) = \boldsymbol{\Phi}_a^{1/2}(\Pi^{\perp}(\boldsymbol{\Phi}_a^{1/2}\boldsymbol{\Psi}_a))\boldsymbol{\Phi}_a^{1/2}$. And the covariance matrix of the target and reflection height in the DOA stage can be expressed as

$$\mathrm{cov}^{(a)}(\hat{\mathbf{u}}_a, \hat{\mathbf{h}}_a) = \mathbf{P}_1\boldsymbol{\Phi}_a^{1/2}(\Pi^{\perp}(\boldsymbol{\Phi}_a^{1/2}\boldsymbol{\Psi}_a))\boldsymbol{\Phi}_a^{1/2}\mathbf{P}_1^{\mathrm{T}}, \tag{55}$$

where $\mathbf{P}_1 = \begin{bmatrix}\mathbf{I}_3 & \mathbf{0}_{3\times1} & \mathbf{0}_{3\times M} \\ \mathbf{0}_{M\times3} & \mathbf{0}_{M\times1} & \mathbf{I}_M\end{bmatrix}$. According to the projection matrix property [34], we have

$\Pi(\boldsymbol{\Phi}_a^{1/2}\boldsymbol{\Psi}_a) = \Pi(\boldsymbol{\Phi}_a^{1/2}\boldsymbol{\psi}_2^{(a)}) + \Pi(\Pi^{\perp}(\boldsymbol{\Phi}_a^{1/2}\boldsymbol{\psi}_2^{(a)})\boldsymbol{\Phi}_a^{1/2}\boldsymbol{\psi}_1^{(a)})$.

After some algebra, we arrive at

$$\begin{aligned}&\Pi(\boldsymbol{\Phi}_a^{1/2}\boldsymbol{\Psi}_a) \\ &= \Pi(\boldsymbol{\Phi}_a^{1/2}\boldsymbol{\psi}_2^{(a)}) \\ &\quad + \frac{\Pi^{\perp}(\boldsymbol{\Phi}_a^{1/2}\boldsymbol{\psi}_2^{(a)})\boldsymbol{\Phi}_a^{1/2}\boldsymbol{\psi}_1^{(a)}(\boldsymbol{\psi}_1^{(a)})^{\mathrm{T}}\boldsymbol{\Phi}_a^{1/2}\Pi^{\perp}(\boldsymbol{\Phi}_a^{1/2}\boldsymbol{\psi}_2^{(a)})}{(\boldsymbol{\psi}_1^{(a)})^{\mathrm{T}}\boldsymbol{\Phi}_a^{1/2}\Pi^{\perp}(\boldsymbol{\Phi}_a^{1/2}\psi_2^{(a)})\boldsymbol{\Phi}_a^{1/2}\boldsymbol{\psi}_1^{(a)}}.\end{aligned} \tag{56}$$

Substituting (56) into (55) and combining $\boldsymbol{\psi}_1^{(a)} = \mathbf{P}_1^{\mathrm{T}}\bar{\boldsymbol{\Lambda}}\xi_2$ yield

$$\begin{aligned}&\mathrm{cov}^{(a)}(\hat{\mathbf{u}}_a, \hat{\mathbf{h}}_a) \\ &= \mathbf{P}_1\boldsymbol{\Phi}_a^{1/2}(\Pi^{\perp}(\boldsymbol{\Phi}_1^{1/2}\boldsymbol{\psi}_2^{(a)}))\boldsymbol{\Phi}_a^{1/2}\mathbf{P}_1^{\mathrm{T}} - \mathbf{P}_1\boldsymbol{\Phi}_a^{1/2} \\ &\times \frac{(\Pi^{\perp}(\boldsymbol{\Phi}_a^{1/2}\boldsymbol{\psi}_2^{(a)}))\boldsymbol{\Phi}_a^{1/2}(\mathbf{P}_1^{\mathrm{T}}\bar{\boldsymbol{\Lambda}}_1\boldsymbol{\xi}_2)^{\mathrm{T}}\boldsymbol{\Phi}_a^{1/2}(\Pi^{\perp}(\boldsymbol{\Phi}_a^{1/2}\boldsymbol{\psi}_2^{(a)}))}{(\mathbf{P}_1^{\mathrm{T}}\bar{\boldsymbol{\Lambda}}_1\boldsymbol{\xi}_2)^{\mathrm{T}}\boldsymbol{\Phi}_a^{1/2}(\Pi^{\perp}(\boldsymbol{\Phi}_a^{1/2}\boldsymbol{\psi}_2^{(a)}))\boldsymbol{\Phi}_a^{1/2}(\mathbf{P}_1^{\mathrm{T}}\bar{\boldsymbol{\Lambda}}_1\boldsymbol{\xi}_2)},\end{aligned} \tag{57}$$

where $\bar{\boldsymbol{\Lambda}}_1 = blkdiag(\boldsymbol{\Lambda}_1, \mathbf{0}_{M\times M})$. Comparing (31) and (57), we need to prove $\mathbf{P}_1\boldsymbol{\Phi}_a^{1/2}(\Pi^{\perp}(\Phi_1^{1/2}\boldsymbol{\psi}_2^{(a)}))\boldsymbol{\Phi}_a^{1/2}\mathbf{P}_1^{\mathrm{T}} = \mathbf{CRLB}_1^{(a)}$.

Define the matrix

$$\boldsymbol{\Gamma} = \begin{bmatrix}\boldsymbol{\Gamma}_{11} & \mathbf{0}_{4\times M} \\ \mathbf{0}_{M\times3} & \mathbf{I}_M\end{bmatrix} \in \mathbb{R}^{(4+M)\times(3+M)}, \tag{58}$$

where $\boldsymbol{\Gamma}_{11} = [\mathbf{I}_3, 2\hat{\mathbf{u}}_a]^{\mathrm{T}}$. Based on $\boldsymbol{\Gamma}^{\mathrm{T}}\boldsymbol{\psi}_2^{(a)} = \mathbf{0}_{(3+M)\times1}$, we have $(\Phi_a^{-1/2}\boldsymbol{\Gamma})^{\mathrm{T}}(\boldsymbol{\Phi}_a^{1/2}\boldsymbol{\psi}_2^{(a)}) = \mathbf{0}_{(3+M)\times1}$. And we can obtain $rank(\boldsymbol{\Phi}_a^{1/2}\boldsymbol{\psi}_2^{(a)}) = 1$ and $rank(\boldsymbol{\Phi}_a^{-1/2}\boldsymbol{\Gamma}) = 3+M$. Thus, we can obtain

$$\Pi(\boldsymbol{\Phi}_a^{-1/2}\boldsymbol{\Gamma}) = \Pi^{\perp}(\boldsymbol{\Phi}_a^{1/2}\psi_2^{(a)}). \tag{59}$$

Substituting (59) into $\mathbf{P}_1\boldsymbol{\Phi}_a^{1/2}(\Pi^{\perp}(\boldsymbol{\Phi}_1^{1/2}\boldsymbol{\psi}_2^{(a)}))\boldsymbol{\Phi}_a^{1/2}\mathbf{P}_1^{\mathrm{T}}$ yields

$$\mathbf{P}_1\boldsymbol{\Phi}_a^{1/2}(\Pi^{\perp}(\boldsymbol{\Phi}_1^{1/2}\boldsymbol{\psi}_2^{(a)}))\boldsymbol{\Phi}_a^{1/2}\mathbf{P}_1^{\mathrm{T}} = \mathbf{P}_1\boldsymbol{\Gamma}(\boldsymbol{\Gamma}^{\mathrm{T}}\boldsymbol{\Phi}_a^{-1}\boldsymbol{\Gamma})^{-1}\boldsymbol{\Gamma}^{\mathrm{T}}\mathbf{P}_1^{\mathrm{T}}. \tag{60}$$

Combining $\mathbf{P}_1\boldsymbol{\Gamma} = \mathbf{I}_{(3+M)}$, we can rewrite (60) as $\mathbf{P}_1\boldsymbol{\Gamma}(\boldsymbol{\Gamma}^{\mathrm{T}}\boldsymbol{\Phi}_a^{-1}\Gamma)^{-1}\boldsymbol{\Gamma}^{\mathrm{T}}\mathbf{P}_1^{\mathrm{T}} = (\boldsymbol{\Gamma}^{\mathrm{T}}\boldsymbol{\Phi}_a^{-1}\boldsymbol{\Gamma})^{-1}$.

Therefore, we need to prove $(\boldsymbol{\Gamma}^{\mathrm{T}}\boldsymbol{\Phi}_a^{-1}\boldsymbol{\Gamma})^{-1} = \mathbf{CRLB}_1^{(a)}$. According to the inverse rule [30] of the block matrix, we can rewrite $\mathbf{W}_a$ as

$$\mathbf{W}_a = \begin{bmatrix}(\mathbf{C}_1\mathbf{Q}_{\mathbf{z}_1}\mathbf{C}_1^{\mathrm{T}})^{-1} & -\mathbf{C}_1^{-\mathrm{T}}\mathbf{Q}_{\mathbf{z}_1}^{-1}\mathbf{C}_1^{-1}\mathbf{C}_2 \\ -\mathbf{C}_2^{\mathrm{T}}\mathbf{C}_1^{-\mathrm{T}}\mathbf{Q}_{\mathbf{z}_1}^{-1}\mathbf{C}_1^{-1} & \mathbf{Q}_{\mathbf{h}}^{-1} + \mathbf{C}_2^{\mathrm{T}}\mathbf{C}_1^{-\mathrm{T}}\mathbf{Q}_{\mathbf{z}_1}^{-1}\mathbf{C}_1^{-1}\mathbf{C}_2\end{bmatrix}. \tag{61}$$

With some algebra, we arrive at (62), as shown at the bottom of the next page, According to (19), the following relationship can be obtained.

$$\mathbf{G}_a(f(\hat{\mathbf{u}}_a, \hat{\mathbf{h}}_a), \hat{\mathbf{h}}_a)\boldsymbol{\eta}_a(\hat{\mathbf{u}}_a) = \mathbf{y}_a(f(\boldsymbol{\Theta}_a, \hat{\mathbf{h}}_a), \hat{\mathbf{h}}_a), \tag{63}$$

where $\mathbf{z}_1 = f(\hat{\mathbf{u}}_a, \hat{\mathbf{h}}_a)$ represents the non-linear relationship between DOA measurements, the target, reflection height. The derivation of both sides of (63) with respect to $\hat{\mathbf{u}}_a$ and $\hat{\mathbf{h}}_a$ gives

$$\begin{aligned}\mathbf{C}_1(\partial\mathbf{z}_1/\partial\hat{\mathbf{u}}_a^{\mathrm{T}}) &= \mathbf{G}_a(\partial\boldsymbol{\eta}_a/\partial\hat{\mathbf{u}}_a^{\mathrm{T}}) \\ &\Rightarrow (\partial\mathbf{z}_1/\partial\hat{\mathbf{u}}_a^{\mathrm{T}}) = \mathbf{C}_1^{-1}\mathbf{G}_a(\partial\boldsymbol{\eta}_a/\partial\hat{\mathbf{u}}_a^{\mathrm{T}})\end{aligned} \tag{64}$$

$$\begin{aligned}, \mathbf{C}_1(\partial\mathbf{z}_1/\partial\hat{\mathbf{h}}_a^{\mathrm{T}}) + \mathbf{C}_2 &= \mathbf{0}_{2M\times M} \\ &\Rightarrow (\partial\mathbf{z}_1/\partial\hat{\mathbf{h}}_a^{\mathrm{T}}) = -\mathbf{C}_1^{-1}\mathbf{C}_2.\end{aligned} \tag{65}$$

Substituting (64) and (65) into (62), we proved $\mathrm{cov}^{(a)}(\hat{\mathbf{u}}_a, \hat{\mathbf{h}}_a) = \mathbf{CRLB}_2^{(a)}$.

B. TDOA STAGE

1) PROPOSED ALGORITHM OF TDOA STAGE

In TDOA stage, $\hat{\mathbf{u}}_a$ and $\hat{\mathbf{h}}_a$ from DOA stage are considered as measurements with errors. Therefore, we use $\hat{\mathbf{u}}_a$, $\hat{\mathbf{h}}_a$ and $\mathbf{r}$ to jointly estimate target position and ionosphere reflection height in TDOA stage essentially.

Substituting measurements into (25) yields

$$\boldsymbol{\varepsilon}_t = \mathbf{y}_t - \mathbf{G}_t\boldsymbol{\eta}_t. \tag{66}$$

Similar to DOA stage, performing first-order Taylor expansion of $\mathbf{y}_t$ and $\mathbf{G}_t$ yields

$$\begin{cases}\mathbf{y}_t \approx \mathbf{y}_t^o + \mathbf{A}_3\mathbf{n_r} + \mathbf{A}_4(\Delta\hat{\mathbf{h}}_a) + \mathbf{A}_5(\Delta\hat{\mathbf{u}}_a) \\ \mathbf{G}_t \approx \mathbf{G}_t^o + \sum_{d_3=1}^{M-1} < \mathbf{r} >_{d_3} \mathbf{B}_{3,d_3} \\ \quad + \sum_{d_4=1}^{M} < \hat{\mathbf{h}}_a >_{d_4} \mathbf{B}_{4,d_4} + \sum_{d_5=1}^{3} < \hat{\mathbf{u}}_a >_{d_5} \mathbf{B}_{5,d_5}\end{cases}, \tag{67}$$

where

$$\begin{cases} \mathbf{A}_3 = (\partial \mathbf{y}_t/\partial \mathbf{r}^{\mathrm{T}}), \mathbf{B}_{3,d_3} = (\partial \mathbf{G}_t/\partial < \mathbf{r} >_{d_3}) \\ \mathbf{A}_4 = (\partial \mathbf{y}_t/\partial \mathbf{h}^{\mathrm{T}}), \mathbf{B}_{4,d_4} = (\partial \mathbf{G}_t/\partial < \mathbf{h} >_{d_4}) \\ \mathbf{A}_5 = (\partial \mathbf{y}_t/\partial \mathbf{u}^{\mathrm{T}}), \mathbf{B}_{5,d_5} = (\partial \mathbf{G}_t/\partial < \mathbf{u} >_{d_5}) \end{cases}. \quad (68)$$

Substituting (67) into (66) gives

$$\boldsymbol{\varepsilon}_t \approx \mathbf{C}_3\mathbf{n}_{\mathbf{r}} + \mathbf{C}_4(\Delta\hat{\mathbf{h}}) + \mathbf{C}_5(\Delta\hat{\mathbf{u}}), \quad (69)$$

where $\Delta\hat{\mathbf{u}}$ and $\Delta\hat{\mathbf{h}}$ denote the estimation errors in DOA stage of the target and ionosphere reflection height, respectively.

$$\begin{aligned} \mathbf{C}_3 &= (\mathbf{A}_3 - [\mathbf{B}_{3,1}\boldsymbol{\eta}_t, \mathbf{B}_{3,2}\boldsymbol{\eta}_t, \ldots, \mathbf{B}_{3,(M-1)}\boldsymbol{\eta}_t]) \\ \mathbf{C}_4 &= (\mathbf{A}_4 - [\mathbf{B}_{4,1}\boldsymbol{\eta}_t, \mathbf{B}_{4,2}\boldsymbol{\eta}_t, \ldots, \mathbf{B}_{4,M}\boldsymbol{\eta}_t]) \\ \mathbf{C}_5 &= (\mathbf{A}_5 - [\mathbf{B}_{5,1}\boldsymbol{\eta}_t, \mathbf{B}_{5,2}\boldsymbol{\eta}_t, \mathbf{B}_{5,3}\boldsymbol{\eta}_t]). \end{aligned} \quad (70)$$

From (2), we only use the first-two dimensions of $\hat{\mathbf{u}}_a$ and $\Delta\hat{\mathbf{u}}_a$. We thus define vectors $\hat{\bar{\boldsymbol{u}}}_a = [\hat{\mathbf{u}}_{a,x}, \hat{\mathbf{u}}_{a,y}]^{\mathrm{T}}$ and $\Delta\hat{\bar{\boldsymbol{u}}}_a = [\Delta\hat{\mathbf{u}}_{a,x}, \Delta\hat{\mathbf{u}}_{a,y}]^{\mathrm{T}}$.

Therefore, the optimization problem in TDOA stage can be formulated as

$$\begin{cases} \min\limits_{\tilde{\boldsymbol{\eta}}_t} \mathrm{J}_t(\tilde{\boldsymbol{\eta}}_t) = (\tilde{\mathbf{y}}_t - \tilde{\mathbf{G}}_t\tilde{\boldsymbol{\eta}}_t)^{\mathrm{T}}\mathbf{W}_t(\tilde{\mathbf{y}}_t - \tilde{\mathbf{G}}_t\tilde{\boldsymbol{\eta}}_t) \\ \text{s.t. } \tilde{\boldsymbol{\eta}}_t^{\mathrm{T}}\tilde{\boldsymbol{\Lambda}}_1\tilde{\boldsymbol{\eta}}_t - R_e^2 = 0 \\ \tilde{\boldsymbol{\eta}}_t^{\mathrm{T}}\tilde{\boldsymbol{\Lambda}}_2\tilde{\boldsymbol{\eta}}_t + \boldsymbol{\gamma}_1^{\mathrm{T}}\tilde{\boldsymbol{\eta}}_t = 0, \end{cases} \quad (71)$$

where

$$\tilde{\mathbf{y}}_t = \begin{bmatrix} \mathbf{y}_t \\ \hat{\bar{\boldsymbol{u}}}_a \\ \hat{\mathbf{h}}_a \end{bmatrix} \in \mathbb{R}^{(2M+1)\times 1}, \tilde{\boldsymbol{\eta}}_t = \begin{bmatrix} \boldsymbol{\eta}_t \\ \hat{\mathbf{h}}_a \end{bmatrix} \in \mathbb{R}^{(4+M)\times 1}$$

$$\tilde{\mathbf{G}}_t = \left[\begin{array}{cc:c} \multicolumn{2}{c:}{\mathbf{G}_t} & \mathbf{0}_{(M+1)\times M} \\ \mathbf{I}_2 & \mathbf{0}_{2\times 2} & \\ \hdashline \multicolumn{2}{c:}{\mathbf{0}_{M\times 4}} & \mathbf{I}_M \end{array}\right], \quad (72)$$

and $\mathbf{W}_t$ is given as (73), shown at the bottom of the next page.

Here, $\mathrm{cov}^{(a)}(\hat{\mathbf{u}}_a) = \boldsymbol{\Sigma}_1\mathrm{cov}^{(a)}(\hat{\bar{\boldsymbol{u}}}_a)\boldsymbol{\Sigma}_1^{\mathrm{T}}$.

Like the DOA stage, we construct the following Lagrange function:

$$\mathrm{L}_t(\tilde{\boldsymbol{\eta}}_t, \boldsymbol{\lambda}_t) = \mathrm{J}_t(\tilde{\boldsymbol{\eta}}_t) + \boldsymbol{\lambda}_t^{\mathrm{T}}\mathrm{g}(\tilde{\boldsymbol{\eta}}_t), \quad (74)$$

where $\boldsymbol{\lambda}_t = [\lambda_1^{(t)}, \lambda_2^{(t)}]^{\mathrm{T}}$ is the Lagrange multiplier and $\mathrm{g}(\tilde{\boldsymbol{\eta}}_t) = [g_1(\tilde{\boldsymbol{\eta}}_t), g_2(\tilde{\boldsymbol{\eta}}_t)]^{\mathrm{T}}$, $g_1(\tilde{\boldsymbol{\eta}}_t) = \tilde{\boldsymbol{\eta}}_t^{\mathrm{T}}\tilde{\boldsymbol{\Lambda}}_1\tilde{\boldsymbol{\eta}}_t - R_e^2$ and $g_2(\tilde{\boldsymbol{\eta}}_t) = \tilde{\boldsymbol{\eta}}_t^{\mathrm{T}}\tilde{\boldsymbol{\Lambda}}_2\tilde{\boldsymbol{\eta}}_t + \boldsymbol{\gamma}_1^{\mathrm{T}}\tilde{\boldsymbol{\eta}}_t$. $\tilde{\boldsymbol{\eta}}_t, \boldsymbol{\lambda}_t$ need to satisfy the following necessary conditions to take the optimal values:

$$\begin{aligned} \tilde{\mathrm{L}}_{\tilde{\boldsymbol{\eta}}_t}(\tilde{\boldsymbol{\eta}}_t, \boldsymbol{\lambda}_t) &= \partial \mathrm{L}_t(\tilde{\boldsymbol{\eta}}_t, \boldsymbol{\lambda}_t)/\partial\tilde{\boldsymbol{\eta}}_t \\ &= \tilde{\mathrm{J}}_t(\tilde{\boldsymbol{\eta}}_t) + \left(\tilde{\mathbf{g}}(\tilde{\boldsymbol{\eta}}_t)\right)^{\mathrm{T}}\boldsymbol{\lambda}_t = \mathbf{0}_{(4+M)\times 1} \\ \tilde{\mathrm{L}}_{\boldsymbol{\lambda}_t}(\tilde{\boldsymbol{\eta}}_t, \boldsymbol{\lambda}_t) &= \partial \mathrm{L}_t(\tilde{\boldsymbol{\eta}}_t, \boldsymbol{\lambda}_t)/\partial\boldsymbol{\lambda}_t = g(\tilde{\boldsymbol{\eta}}_t) = \mathbf{0}_{2\times 1}, \end{aligned} \quad (75)$$

where $\tilde{\mathbf{g}}(\tilde{\boldsymbol{\eta}}_t) = \partial \mathbf{g}(\tilde{\boldsymbol{\eta}}_t)/\partial\tilde{\boldsymbol{\eta}}_t^{\mathrm{T}} = [(2\tilde{\boldsymbol{\eta}}_t^{\mathrm{T}}\tilde{\boldsymbol{\Lambda}}_1)^{\mathrm{T}}, (2\tilde{\boldsymbol{\eta}}_t^{\mathrm{T}}\tilde{\boldsymbol{\Lambda}}_2 + \boldsymbol{\gamma}_1^{\mathrm{T}})^{\mathrm{T}}]^{\mathrm{T}}$ and $\tilde{\mathrm{J}}_t(\tilde{\boldsymbol{\eta}}_t) = \partial \mathrm{J}_t(\tilde{\boldsymbol{\eta}}_t)/\partial\tilde{\boldsymbol{\eta}}_t = 2\tilde{\mathbf{G}}_t\mathbf{W}_t(\tilde{\mathbf{G}}_t\tilde{\boldsymbol{\eta}}_t - \tilde{\mathbf{y}}_t)$. Therefore, the corresponding general penalty function is given as [31]

$$\begin{aligned} \mathrm{P}_t(\tilde{\boldsymbol{\eta}}_t, \boldsymbol{\lambda}_t) = L(\tilde{\boldsymbol{\eta}}_t, \boldsymbol{\lambda}_t) + (\chi^{(t)} + \mu^{(t)}||\boldsymbol{\lambda}_t||^2)||\mathbf{g}(\tilde{\boldsymbol{\eta}}_t)||^2/2 \\ + ||\mathbf{M}_t(\tilde{\boldsymbol{\eta}}_t)\tilde{\mathrm{L}}_t(\tilde{\boldsymbol{\eta}}_t, \boldsymbol{\lambda}_t)||^2/2, \end{aligned} \quad (76)$$

where $\chi^{(t)} > 0$ is the penalty factor and $\mu^{(t)} \geq 0$ is some fixed scalar. $\mathbf{M}_t(\tilde{\boldsymbol{\eta}}_t)$ is set to $(\tilde{\mathbf{g}}(\tilde{\boldsymbol{\eta}}_t)(\tilde{\mathbf{g}}(\tilde{\boldsymbol{\eta}}_t))^{\mathrm{T}})^{-1}\tilde{\mathbf{g}}(\tilde{\boldsymbol{\eta}}_t)$. Similar to DOA stage, main steps of the proposed algorithm in TDOA stage are shown in TABLE 3.

TABLE 3. Main steps of tdoa stage.

Step 1	Let $k=0$ and choose appropriate $\delta^{(t)} > 0$, $\chi^{(t)} > 0$, and $\mu^{(t)} \geq 0$. Set $\hat{\tilde{\boldsymbol{\eta}}}_t^{(0)} = \hat{\tilde{\boldsymbol{\eta}}}_a$ and calculate $\hat{\boldsymbol{\lambda}}_t^{(0)}$ based on (77). $\hat{\boldsymbol{\lambda}}_t^{(0)} = -(1+\mu^{(t)}\,\|\,\mathbf{g}(\hat{\tilde{\boldsymbol{\eta}}}_t^{(0)})\|^2)^{-1}(\mathbf{g}(\hat{\tilde{\boldsymbol{\eta}}}_t^{(0)}) + \mathbf{M}_t(\hat{\tilde{\boldsymbol{\eta}}}_t^{(0)})\tilde{\mathrm{J}}(\hat{\tilde{\boldsymbol{\eta}}}_t^{(0)}))$.(77)
Step 2	Calculate $\Delta\tilde{\boldsymbol{\eta}}_t^{(k)}$ and $\Delta\boldsymbol{\lambda}_t^{(k)}$ based on (78). $\begin{bmatrix} \Delta\tilde{\boldsymbol{\eta}}_t^{(k)} \\ \Delta\boldsymbol{\lambda}_t^{(k)} \end{bmatrix} = \begin{bmatrix} \tilde{\tilde{\mathrm{L}}}_t(\tilde{\boldsymbol{\eta}}_t^{(k)}, \bar{\boldsymbol{\lambda}}_t^{(k)}) & (\tilde{\mathbf{g}}(\tilde{\boldsymbol{\eta}}_t^{(k)}))^{\mathrm{T}} \\ \tilde{\mathbf{g}}(\tilde{\boldsymbol{\eta}}_t^{(k)}) & \mathbf{0}_{2\times 2} \end{bmatrix}^{-1} \begin{bmatrix} \dot{\mathrm{L}}_2(\tilde{\boldsymbol{\eta}}_t^{(k)}, \bar{\boldsymbol{\lambda}}_t^{(k)}) \\ \mathbf{g}(\tilde{\boldsymbol{\eta}}_t^{(k)}) \end{bmatrix}$ (78) Where $\tilde{\tilde{\mathrm{L}}}_t(\tilde{\boldsymbol{\eta}}_t^{(k)}, \bar{\boldsymbol{\lambda}}_t^{(k)}) = 2\tilde{\mathbf{G}}_t^{\mathrm{T}}\mathbf{W}_t\tilde{\mathbf{G}}_t + 2\lambda_1^{(t)}\tilde{\boldsymbol{\Lambda}}_1 + 2\lambda_2^{(t)}\tilde{\boldsymbol{\Lambda}}_2$.
Step 3	Update $\hat{\tilde{\boldsymbol{\eta}}}_t^{(k+1)} = \hat{\tilde{\boldsymbol{\eta}}}_t^{(k)} + \delta_{t1}^{(k)}\Delta\hat{\tilde{\boldsymbol{\eta}}}_t^{(k)}$ and $\hat{\boldsymbol{\lambda}}_t^{(k+1)} = \hat{\boldsymbol{\lambda}}_t^{(k)} + \delta_{t2}^{(k)}\Delta\hat{\boldsymbol{\lambda}}_t^{(k)}$. $\delta_{t1}^{(k)}$ and $\delta_{t2}^{(k)}$ are step sizes.
Step 4	Calculate $\hat{\boldsymbol{\lambda}}_t^{(k+1)}$ based on (79). $\hat{\boldsymbol{\lambda}}_t^{(k+1)} = -(1+\mu_1^{(t)}\,\|\,\mathbf{g}(\hat{\tilde{\boldsymbol{\eta}}}_t^{(k+1)})\|^2)^{-1}(\mathbf{g}(\hat{\tilde{\boldsymbol{\eta}}}_t^{(k+1)}) + \mathbf{M}_t(\hat{\tilde{\boldsymbol{\eta}}}_t^{(k+1)})\tilde{\mathrm{J}}(\hat{\tilde{\boldsymbol{\eta}}}_t^{(k+1)}))$ (79)
Step 5	Let $k=k+1$ and calculate $\mathrm{P}_t(\hat{\tilde{\boldsymbol{\eta}}}_t^{(k)}, \hat{\boldsymbol{\lambda}}_t^{(k)})$ based on (76).
Step 6	If $(|\,\mathrm{P}_t(\hat{\tilde{\boldsymbol{\eta}}}_t^{(k)}, \hat{\boldsymbol{\lambda}}_t^{(t)}) - \mathrm{P}_t(\hat{\tilde{\boldsymbol{\eta}}}_t^{(k-1)}, \hat{\boldsymbol{\lambda}}_t^{(k-1)})\,|\,/\,|\,\mathrm{P}_t(\hat{\tilde{\boldsymbol{\eta}}}_t^{(k-1)}, \hat{\boldsymbol{\lambda}}_t^{(k-1)})\,|) < \delta^{(t)}$, then stop the iteration. If not, go to Step 2.
Step 7	Target position and ionosphere reflection height estimates are given as $\hat{\mathbf{u}} = \hat{\tilde{\boldsymbol{\eta}}}_t^{(k)}(1:3), \hat{\mathbf{h}} = \hat{\tilde{\boldsymbol{\eta}}}_t^{(k)}(4:end)$. (80)

The main steps of the DOA/TDOA localization algorithm can be obtained by connecting the steps shown in TABLE 2 and TABLE 3. The corresponding detailed flow-chart graph of the proposed algorithm is exhibited in FIGURE 2.

2) PERFORMANCE ANALYSIS OF TDOA STAGE

This subsection proves that the accuracy of TDOA stage can reach $\mathbf{CRLB}_2$. The estimation error is defined as $\Delta\tilde{\boldsymbol{\eta}}_t = \hat{\tilde{\boldsymbol{\eta}}}_t - \tilde{\boldsymbol{\eta}}_t^o$, where $\hat{\tilde{\boldsymbol{\eta}}}_t$ is the estimation result and $\tilde{\boldsymbol{\eta}}_t^o$ is the true value.

Performing first-order perturbation analysis, $\Delta\tilde{\boldsymbol{\eta}}_t$ is the optimal solution of the following problem:

$$\begin{cases} \min\limits_{\Delta\tilde{\boldsymbol{\eta}}_t} \left(\tilde{\mathbf{G}}_t\Delta\tilde{\boldsymbol{\eta}}_t - \begin{bmatrix} \boldsymbol{\varepsilon}_t \\ \Delta\tilde{\boldsymbol{\eta}}_a(1:2) \\ \Delta\tilde{\boldsymbol{\eta}}_a(4:end) \end{bmatrix}\right)^{\mathrm{T}} \mathbf{W}_a \left(\tilde{\mathbf{G}}_t\Delta\tilde{\boldsymbol{\eta}}_a - \begin{bmatrix} \boldsymbol{\varepsilon}_t \\ \Delta\tilde{\boldsymbol{\eta}}_a(1:2) \\ \Delta\tilde{\boldsymbol{\eta}}_a(4:end) \end{bmatrix}\right) \\ \text{s.t.} \quad (\Delta\tilde{\boldsymbol{\eta}}_t)^{\mathrm{T}}\tilde{\boldsymbol{\Lambda}}_1\tilde{\boldsymbol{\eta}}_t^o = 0 \\ \qquad (\Delta\tilde{\boldsymbol{\eta}}_t)^{\mathrm{T}}(2\tilde{\boldsymbol{\Lambda}}_2\tilde{\boldsymbol{\eta}}_t^o + \boldsymbol{\gamma}_1) = 0. \end{cases} \quad (81)$$

$$\boldsymbol{\Gamma}^{\mathrm{T}}\boldsymbol{\Phi}_a^{-1}\boldsymbol{\Gamma} = \begin{bmatrix} (\mathbf{C}_1^{-1}\mathbf{G}_1\boldsymbol{\Gamma}_{11})^{\mathrm{T}}\mathbf{Q}_{\mathbf{z}_1}^{-1}(\mathbf{C}_1^{-1}\mathbf{G}_1\Gamma_{11}) & -(\mathbf{C}_1^{-1}\mathbf{G}_1\boldsymbol{\Gamma}_{11})^{\mathrm{T}}\mathbf{Q}_{\mathbf{z}_1}^{-1}\left(\mathbf{C}_1^{-1}\mathbf{C}_2\right) \\ -(\mathbf{C}_1^{-1}\mathbf{C}_2)^{\mathrm{T}}\mathbf{Q}_{\mathbf{z}_1}^{-1}(\mathbf{C}_1^{-1}\mathbf{G}_1\boldsymbol{\Gamma}_{11}) & \mathbf{Q}_{\mathbf{h}}^{-1} + (\mathbf{C}_1^{-1}\mathbf{C}_2)^{\mathrm{T}}\mathbf{Q}_{\mathbf{z}_1}^{-1}(\mathbf{C}_1^{-1}\mathbf{C}_2) \end{bmatrix} \quad (62)$$

And $\Delta\tilde{\boldsymbol{\eta}}_t$ can be given as

$$\Delta\tilde{\boldsymbol{\eta}}_t = (\mathbf{I}_{4+M} - \boldsymbol{\Phi}_t\boldsymbol{\Psi}_t(\boldsymbol{\Psi}_t^{\mathrm{T}}\boldsymbol{\Phi}_t\boldsymbol{\Psi}_t)^{-1}\boldsymbol{\Psi}_t^{\mathrm{T}})\boldsymbol{\Phi}_t\tilde{\mathbf{G}}_t^{\mathrm{T}} \mathbf{W}_t[\boldsymbol{\varepsilon}_t^{\mathrm{T}}, \Delta\tilde{\boldsymbol{\eta}}_a(1:2))^{\mathrm{T}}, (\Delta\tilde{\boldsymbol{\eta}}_a(4:end))^{\mathrm{T}}]^{\mathrm{T}} \quad (82)$$

where $\boldsymbol{\Psi}_t = [\boldsymbol{\psi}_1^{(t)}, \boldsymbol{\psi}_2^{(t)}] = [\tilde{\boldsymbol{\Lambda}}_1\tilde{\boldsymbol{\eta}}_t^o, 2\tilde{\boldsymbol{\Lambda}}_2\tilde{\boldsymbol{\eta}}_t^o + \boldsymbol{\gamma}_1]$ and $\boldsymbol{\Phi}_t = (\tilde{\mathbf{G}}_t^{\mathrm{T}}\mathbf{W}_t\tilde{\mathbf{G}}_t)^{-1}$. Therefore, the covariance matrix of $\hat{\mathbf{u}}$ and $\hat{\mathbf{h}}$ in TDOA stage is expressed as

$$\mathrm{cov}^{(t)}(\hat{\mathbf{u}}, \hat{\mathbf{h}}) = \mathbf{P}_1\boldsymbol{\Phi}_t^{1/2}(\Pi^{\perp}(\boldsymbol{\Phi}_2^{1/2}\boldsymbol{\Psi}_t))\Phi_t^{1/2}\mathbf{P}_2^{\mathrm{T}}. \quad (83)$$

Similar to (56), we can obtain

$$\Pi(\boldsymbol{\Phi}_t^{1/2}\boldsymbol{\Psi}_t) = \Pi(\boldsymbol{\Phi}_t^{1/2}\boldsymbol{\psi}_2^{(t)}) + \frac{(\Pi^{\perp}(\boldsymbol{\Phi}_t^{1/2}\boldsymbol{\psi}_2^{(t)}))\boldsymbol{\Phi}_3^{1/2}\boldsymbol{\psi}_1^{(t)}(\boldsymbol{\psi}_1^{(t)})^{\mathrm{T}}\boldsymbol{\Phi}_2^{1/2}(\Pi^{\perp}(\boldsymbol{\Phi}_t^{1/2}\boldsymbol{\psi}_2^{(t)}))}{(\boldsymbol{\psi}_1^{(t)})^{\mathrm{T}}\Phi_t^{1/2}(\Pi^{\perp}(\boldsymbol{\Phi}_t^{1/2}\boldsymbol{\psi}_2^{(t)}))\boldsymbol{\Phi}_t^{1/2}\boldsymbol{\psi}_1^{(t)}}. \quad (84)$$

Substituting (84) into (83) and combining $\boldsymbol{\psi}_1^{(t)} = \mathbf{P}_1^{\mathrm{T}}\bar{\boldsymbol{\Lambda}}\xi_2$ give

$$\mathrm{cov}^{(t)}(\hat{\mathbf{u}}, \hat{\mathbf{h}}) = \mathbf{P}_1\boldsymbol{\Phi}_t^{1/2}(\Pi^{\perp}(\boldsymbol{\Phi}_t^{1/2}\boldsymbol{\psi}_2^{(t)}))\Phi_t^{1/2}\mathbf{P}_1^{\mathrm{T}} - \mathbf{P}_1\boldsymbol{\Phi}_t^{1/2} \times \frac{(\Pi^{\perp}(\boldsymbol{\Phi}_t^{1/2}\boldsymbol{\psi}_2^{(t)}))\boldsymbol{\Phi}_t^{1/2}(\mathbf{P}_1^{\mathrm{T}}\bar{\boldsymbol{\Lambda}}\xi_2)^{\mathrm{T}}\boldsymbol{\Phi}_t^{1/2}(\Pi^{\perp}(\boldsymbol{\Phi}_t^{1/2}\boldsymbol{\psi}_2^{(t)}))}{(\mathbf{P}_1^{\mathrm{T}}\bar{\boldsymbol{\Lambda}}\xi_2)^{\mathrm{T}}\boldsymbol{\Phi}_t^{1/2}(\Pi^{\perp}(\boldsymbol{\Phi}_t^{1/2}\boldsymbol{\psi}_2^{(t)}))\boldsymbol{\Phi}_t^{1/2}(\mathbf{P}_1^{\mathrm{T}}\bar{\boldsymbol{\Lambda}}\xi_2)}. \quad (85)$$

And we need to prove $\mathbf{P}_1\boldsymbol{\Phi}_t^{1/2}(\Pi^{\perp}(\boldsymbol{\Phi}_t^{1/2}\boldsymbol{\psi}_2^{(t)}))\boldsymbol{\Phi}_t^{1/2}\mathbf{P}_1^{\mathrm{T}} = \mathbf{CRLB}_1$.

Based on $\boldsymbol{\Gamma}$ and $\boldsymbol{\Phi}_t$, we have $\boldsymbol{\Gamma}^{\mathrm{T}}\boldsymbol{\psi}_2^{(t)} = \mathbf{0}_{(3+M)\times 1}$ and $(\boldsymbol{\Phi}_t^{-1/2}\boldsymbol{\Gamma})^{\mathrm{T}}(\boldsymbol{\Phi}_t^{1/2}\boldsymbol{\psi}_2^{(t)}) = \mathbf{0}_{(3+M)\times 1}$. Because of $rank(\boldsymbol{\Phi}_t^{1/2}\boldsymbol{\psi}_2^{(t)}) = 1$ and $rank(\boldsymbol{\Phi}_t^{-1/2}\boldsymbol{\Gamma}) = 3 + M$, we can obtain

$$\Pi(\boldsymbol{\Phi}_t^{-1/2}\boldsymbol{\Gamma}) = \Pi^{\perp}(\boldsymbol{\Phi}_t^{1/2}\psi_2^{(t)}). \quad (86)$$

Substituting (86) into $\mathbf{P}_1\boldsymbol{\Phi}_t^{1/2}(\Pi^{\perp}(\boldsymbol{\Phi}_t^{1/2}\boldsymbol{\psi}_2^{(t)}))\boldsymbol{\Phi}_t^{1/2}\mathbf{P}_1^{\mathrm{T}}$ yields

$$\mathbf{P}_1\boldsymbol{\Phi}_t^{1/2}(\Pi^{\perp}(\boldsymbol{\Phi}_t^{1/2}\boldsymbol{\psi}_2^{(t)}))\boldsymbol{\Phi}_t^{1/2}\mathbf{P}_1^{\mathrm{T}} = \mathbf{P}_1\boldsymbol{\Gamma}(\boldsymbol{\Gamma}^{\mathrm{T}}\boldsymbol{\Phi}_t^{-1}\boldsymbol{\Gamma})^{-1}\boldsymbol{\Gamma}^{\mathrm{T}}\mathbf{P}_2^{\mathrm{T}}. \quad (87)$$

Comparing (87) and (32), we need to prove $\boldsymbol{\Gamma}^{\mathrm{T}}\boldsymbol{\Phi}_t^{-1}\Gamma = (\mathbf{CRLB}_1)^{-1}$. With some algebra, we can rewrite $\boldsymbol{\Gamma}^{\mathrm{T}}\boldsymbol{\Phi}_t^{-1}\Gamma$ as (88), shown at the bottom of the next page, where $\mathbf{D}_1 = (\mathbf{C}_3\mathbf{Q}_{\mathbf{r}}\mathbf{C}_3^{\mathrm{T}} + \mathbf{C}_4\mathrm{cov}^{(a)}(\hat{\mathbf{h}}_a)\mathbf{C}_4^{\mathrm{T}})^{-1}$, $\mathbf{D}_2 = \mathbf{C}_5\boldsymbol{\Sigma}_1$, $\mathbf{D}_3 = \mathbf{C}_4\mathrm{cov}^{(a)}(\hat{\mathbf{h}}_a)$, $\mathbf{D}_4 = (\mathrm{cov}^{(a)}(\hat{\mathbf{h}}_a) - \mathbf{D}_3^{\mathrm{T}}\mathbf{D}_1\mathbf{D}_3)^{-1}$.

Based on (25), we have

$$\mathbf{G}_t(f(\hat{\mathbf{u}}, \hat{\mathbf{h}}), \hat{\mathbf{h}})\eta_t(\hat{\mathbf{u}}) = \mathbf{y}_t(f(\hat{\mathbf{u}}, \hat{\mathbf{h}}_t), \hat{\mathbf{h}}_t). \quad (89)$$

TABLE 4. Location of station and corresponding ionosphere reflection height.

Station	Longitude (°)	Latitude (°)	Reflection Height (KM)
1	116.23	40.22	340.00
2	112.54	33.00	390.00
3	116.00	29.71	370.00
4	123.47	41.80	310.00
5	114.54	38.04	350.00

The partial derivatives of both sides of (89) with respect to $\hat{\mathbf{u}}$ and $\hat{\mathbf{h}}$ are obtained as

$$\mathbf{C}_5 + \mathbf{C}_3(\partial\mathbf{r}/\partial\hat{\mathbf{u}}^{\mathrm{T}}) = \mathbf{G}_t(\partial\boldsymbol{\eta}_t/\partial\hat{\mathbf{u}}^{\mathrm{T}}) \Rightarrow (\partial\mathbf{r}/\partial\hat{\mathbf{u}}^{\mathrm{T}}) = \mathbf{C}_3^{-1}(\mathbf{G}_t(\partial\boldsymbol{\eta}_t/\partial\hat{\mathbf{u}}^{\mathrm{T}}) - \mathbf{C}_5), \quad (90)$$

$$\mathbf{C}_3(\partial\mathbf{r}/\partial\hat{\mathbf{h}}^{\mathrm{T}}) + \mathbf{C}_4 = \mathbf{0}_{(M-1)\times M} \Rightarrow (\partial\mathbf{r}/\partial\hat{\mathbf{h}}^{\mathrm{T}}) = -\mathbf{C}_3^{-1}\mathbf{C}_4. \quad (91)$$

After some algebra, we can obtain $\partial\boldsymbol{\eta}_t/\partial\hat{\mathbf{u}}^{\mathrm{T}} = \boldsymbol{\Gamma}_{11}$ and

$$(\mathbf{CRLB}_2)^{-1} = (\mathbf{CRLB}_1^{(a)})^{-1} + (\mathbf{CRLB}_1^{(t)})^{-1} - blkdiag(\mathbf{0}_{3\times 3}, \mathbf{Q}_{\mathbf{h}}^{-1}) \quad (92)$$

Combining (88), (90), (91) and (92) yields $\mathrm{cov}^{(t)}(\hat{\mathbf{u}}, \hat{\mathbf{h}}) = \mathbf{CRLB}_2$.

VI. SIMULATIONS

Simulations are performed to verify outperformance of the proposed algorithm. The locations of 5 stations and the corresponding ionosphere reflection height are shown in TABLE 4. $\mathbf{n}_{\boldsymbol{\theta}}$, $\mathbf{n}_{\boldsymbol{\varphi}}$, $\mathbf{n}_{\mathbf{r}}$ and $\mathbf{n}_{\mathbf{h}}$ are assumed to be independent and follow zero-mean Gaussian distribution. The corresponding covariance matrices are $\mathbf{Q}_{\boldsymbol{\theta}} = \sigma_{\boldsymbol{\theta}}^2\mathbf{I}_M$, $\mathbf{Q}_{\boldsymbol{\varphi}} = \sigma_{\boldsymbol{\varphi}}^2\mathbf{I}_M$, $\mathbf{Q}_{\mathbf{r}} = \sigma_{\mathbf{r}}^2\mathbf{R}_{M-1}$ and $\mathbf{Q}_{\mathbf{h}} = \sigma_{\mathbf{h}}^2\mathbf{I}_M$. $\mathbf{R}_{M-1}$ is the $(M-1)\times(M-1)$ matrix with 1 in the diagonal elements and 0.5 otherwise. The positioning accuracy is evaluated using the root mean square error (RMSE), which is defined as

$$RMSE(\hat{\mathbf{u}}) = \sqrt{\sum_{j=1}^{K}||\hat{\mathbf{u}} - \mathbf{u}^o||_2^2/K} \quad RMSE(\hat{\mathbf{h}}) = \sqrt{\sum_{j=1}^{K}||\hat{\mathbf{h}} - \mathbf{h}^o||_2^2/K}, \quad (93)$$

where $K = 5000$ is the number of Monte Carlo experiments. In the simulations, set $\chi^{(a)} = \chi^{(t)} = 10^3$ and $\mu^{(a)} = \mu^{(t)} = 3$. In figures, 'DOA stage' and 'TDOA stage' represent the

$$\mathbf{W}_t = \begin{bmatrix} \mathbf{C}_3\mathbf{Q}_{\mathbf{r}}\mathbf{C}_3^{\mathrm{T}} + \mathbf{C}_4\mathrm{cov}^{(a)}(\hat{\mathbf{h}}_a)\mathbf{C}_4^{\mathrm{T}} + \mathbf{C}_5\mathrm{cov}^{(a)}(\hat{\mathbf{u}})\mathbf{C}_5^{\mathrm{T}} & \mathbf{C}_5\boldsymbol{\Sigma}_1\mathrm{cov}^{(a)}(\hat{\tilde{\boldsymbol{u}}}_a) & \mathbf{C}_4\mathrm{cov}^{(a)}(\hat{\mathbf{h}}_a) \\ (\mathbf{C}_5\boldsymbol{\Sigma}_1\mathrm{cov}^{(a)}(\hat{\tilde{\boldsymbol{u}}}_a))^{\mathrm{T}} & \mathrm{cov}^{(a)}(\hat{\tilde{\boldsymbol{u}}}_a) & \mathbf{0}_{2\times M} \\ (\mathbf{C}_4\mathrm{cov}^{(a)}(\hat{\mathbf{h}}_a))^{\mathrm{T}} & \mathbf{0}_{M\times 2} & \mathrm{cov}^{(a)}(\hat{\mathbf{h}}_a) \end{bmatrix}^{-1}. \quad (73)$$

first and second stages of the proposed algorithm, respectively.

A. EFFECTIVENESS VERIFICATION

This subsection verifies the effectiveness of the proposed method by error probability ellipses.

And the probability is set to 0.5, 0.7 and 0.9, respectively. Target is located at (134°, 34°). And set $\sigma_{\boldsymbol{\theta}} = 0.02$(rad), $\sigma_{\boldsymbol{\varphi}} = 0.03$(rad), $\sigma_{\mathbf{r}} = 1$(KM) and $\sigma_{\mathbf{h}} = 10$(KM). The results are shown in FIGURE 3.

FIGURE 3 shows the scatter plots of estimations of the target and the error ellipse with corresponding probabilities in X-Y plane (a), X-Z plane (b) and Y-Z plane (c). The estimation results are consistent with the ellipse. And the probability corresponds to the area of the ellipse, that is, large probability corresponds to large area ellipse and small probability corresponds to small area ellipse. The effectiveness of the proposed method can be proved by the results shown in FIGURE 3.

B. CONVERGENCE COMPARISON

This subsection compares iteration number of the Lagrange method with the proposed method. The Newton's method [25,26] is used to find the roots in Lagrange method. Set attenuation factor $\alpha = 0.99$ and the maximum number of iterations is fixed to 50. The target is located at (134°, 34°).

FIGURE 4 shows the results of the number of iterations with the variation of DOA measurement noise, and parameters are set as $\sigma_{\boldsymbol{\theta}} = 2\sigma_1$(rad), $\sigma_{\boldsymbol{\varphi}} = 3\sigma_1$(rad), $\sigma_{\mathbf{r}} = 1$(KM) and $\sigma_{\mathbf{h}} = 10$(KM). FIGURE 5 shows the results with the variation of TDOA measurement noise, and parameters are set as $\sigma_{\boldsymbol{\theta}} = 0.01$(rad), $\sigma_{\boldsymbol{\varphi}} = 0.015$(rad), $\sigma_{\mathbf{r}} = 10^2\sigma_2$(KM) and $\sigma_{\mathbf{h}} = 2$(KM). FIGURE 6 shows the results with the variation of reflection height noise and parameters are set as $\sigma_{\boldsymbol{\theta}} = 0.01$(rad), $\sigma_{\boldsymbol{\varphi}} = 0.015$(rad), $\sigma_{\mathbf{r}} = 1$(KM) and $\sigma_{\mathbf{h}} = 5 \times 10^2\sigma_3$(KM).

As can be seen from FIGURE 4 to FIGURE 6, the number of iterations for two methods increases as the noise increases. The proposed method has a smaller number of iterations in both DOA stage and TDOA stage compared to the Lagrange algorithm. This shows that the combining differentiable exact penalty method in this paper can effectively expand the convergence region of the Lagrange algorithm and reduce the number of iterations.

C. POSITIONING PERFORMANCE COMPARISON

This subsection analyzes the positioning performance of the proposed algorithm by simulation. The longitudes and latitudes of the three targets are (134°, 34°), (140°, 36°), and (146°, 40°) respectively. The location of targets and the observation stations are shown in FIGURE 7. The distances and average distances between each target and observation stations are given in TABLE 5.

TABLE 5. Distance between targets and stations.

Distance (KM)	Target 1	Target 2	Target 2
$\mathbf{s}_1^o$	1714.45	2119.85	2509.75
$\mathbf{s}_2^o$	1985.47	2518.68	3047.32
$\mathbf{s}_3^o$	1760.37	2332.06	2927.14
$\mathbf{s}_4^o$	1263.86	1564.48	1896.38
$\mathbf{s}_5^o$	1800.73	2257.87	2698.54
Average distance (KM)	1704.98	2158.59	2615.82

First, the effect of DOA measurement noise on the positioning results is simulated, and parameters are set as $\sigma_{\boldsymbol{\theta}} = 2\sigma_1$(rad), $\sigma_{\boldsymbol{\varphi}} = 3\sigma_1$(rad), $\sigma_{\mathbf{r}} = 1$(KM) and $\sigma_{\mathbf{h}} = 10$(KM). Results of targets and ionosphere height estimation are shown in FIGURE 8, FIGURE 9 and FIGURE 10. The 'Prior RMSE' is calculated by $\mathbf{Q_h}$.

Then the effect of TDOA measurement noise on the positioning results is simulated. Set $\sigma_{\boldsymbol{\theta}} = 0.01$(rad), $\sigma_{\boldsymbol{\varphi}} = 0.015$(rad), $\sigma_{\mathbf{r}} = 10^2\sigma_2$(KM) and $\sigma_{\mathbf{h}} = 2$(KM). FIGURE 11 to FIGURE 13 are the corresponding results.

At last, we simulate the effect of ionosphere reflection height measurement noise. Set $\sigma_{\boldsymbol{\theta}} = 0.01$(rad), $\sigma_{\boldsymbol{\varphi}} = 0.015$(rad), $\sigma_{\mathbf{r}} = 1$(KM) and $\sigma_{\mathbf{h}} = 5 \times 10^2\sigma_3$(KM). Results are show in FIGURE 14 to FIGURE 16.

From FIGURE 8 to FIGURE 16, the accuracy of the target and ionosphere reflection height can achieve the corresponding CRLB in DOA stage and TDOA stage with different noise levels.

In addition, the accuracy of the TDOA stage is higher than that of the DOA stage and achieves the CRLB of hybrid positioning, which indicates that the TDOA stage improves the accuracy by using the results of DOA stage. Through the cooperation of DOA stage and TDOA stage, the localization accuracy is improved, which illustrates the effectiveness of using two stages in short-wave positioning. Comparing $\mathbf{CRLB}_1$ and $\mathbf{CRLB}_2$ in FIGURE 8 to FIGURE 16, we can obtain that the target positioning accuracy can be effectively improved with constraint (2).

From the results of ionosphere reflection height, the estimation accuracy of ionosphere reflection height is higher than that of 'Prior RMSE', which indicates that the joint estimation of target position and ionosphere reflection height will bring gains to the estimation of ionosphere reflection height.

$$\boldsymbol{\Gamma}^{\mathrm{T}}\boldsymbol{\Phi}_2^{-1}\boldsymbol{\Gamma} = \begin{bmatrix} \mathrm{cov}^{(a)}(\hat{\mathbf{u}}) + (\mathbf{C}_3^{-1}(\mathbf{G}_1\boldsymbol{\Gamma}_{11} - \mathbf{C}_5))^{\mathrm{T}}\mathbf{Q}_{\mathbf{r}}^{-1}(\mathbf{C}_3^{-1}(\mathbf{G}_1\boldsymbol{\Gamma}_{11} - \mathbf{C}_5)) & -\boldsymbol{\Gamma}_{11}^{\mathrm{T}}\mathbf{G}_1^{\mathrm{T}}\mathbf{D}_1\mathbf{D}_3\mathbf{D}_4 + \boldsymbol{\Gamma}_{11}^{\mathrm{T}}\tilde{\mathbf{I}}_{4\times 2}\mathbf{D}_2^{\mathrm{T}}\mathbf{D}_1\mathbf{D}_3\mathbf{D}_4 \\ (-\boldsymbol{\Gamma}_{11}^{\mathrm{T}}\mathbf{G}_1^{\mathrm{T}}\mathbf{D}_1\mathbf{D}_3\mathbf{D}_4 + \boldsymbol{\Gamma}_{11}^{\mathrm{T}}\tilde{\mathbf{I}}_{4\times 2}\mathbf{D}_2^{\mathrm{T}}\mathbf{D}_1\mathbf{D}_3\mathbf{D}_4)^{\mathrm{T}} & (\mathrm{cov}^{(a)}(\hat{\mathbf{h}}_a) - \mathbf{D}_3^{\mathrm{T}}\mathbf{D}_1\mathbf{D}_3)^{-1} \end{bmatrix} \quad (88)$$

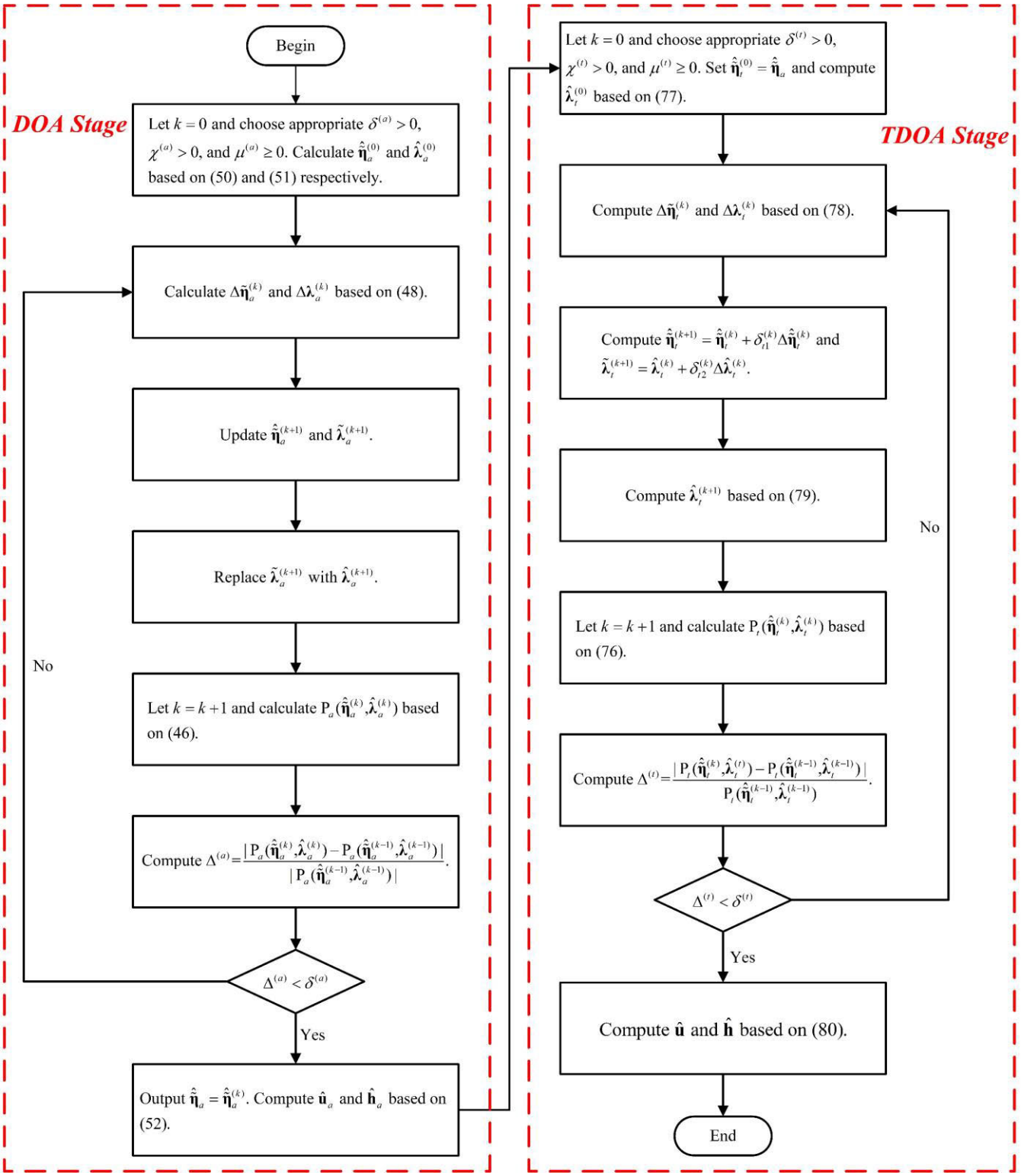

FIGURE 2. Block diagram for the proposed method.

Comparing the results of targets in FIGURE 8 to FIGURE 10, the threshold value of the threshold effect in DOA stage and TDOA stage becomes lower as the distance between the target and the station increases. However, $\mathbf{CRLB}_1$ decreases as the distance between the target and the station increases, which indicates that the positioning accuracy increases as the distance increases. In general, the accuracy of DOA localization and TDOA localization decreases as the distance between the target and the station increases. But the accuracy is also related to the distribution of stations.

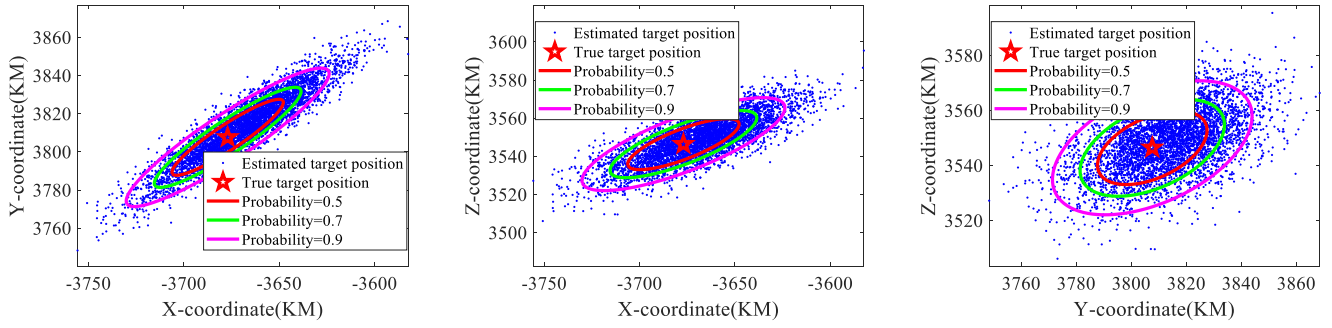

(a) X-Y plane (b) X-Z plane (c) Y-Z plane

FIGURE 3. Estimations and the corresponding error ellipse.

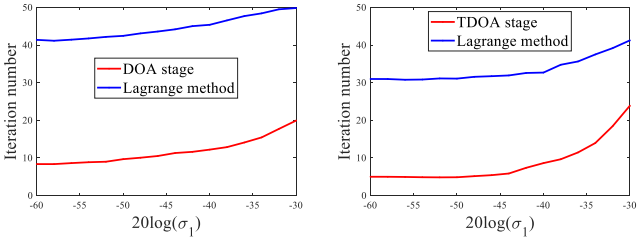

(a) DOA stage (b) TDOA stage

FIGURE 4. Number of iterations varies with σ_1.

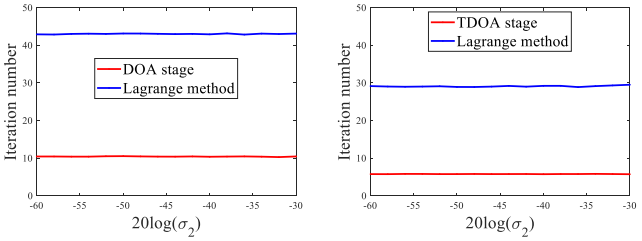

(a) DOA stage (b) TDOA stage

FIGURE 5. Number of iterations varies with σ_2.

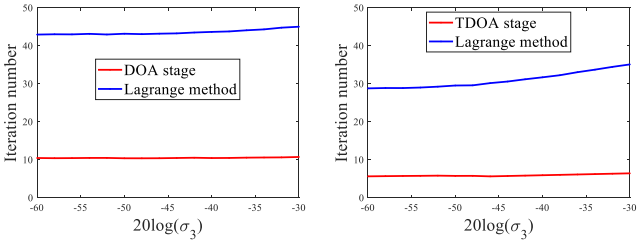

(a) DOA stage (b) TDOA stage

FIGURE 6. Number of iterations varies with σ_3.

D. ROBUSTNESS ANALYSIS

This subsection simulates the robustness of the proposed algorithm to target locations. 30 targets were randomly selected in the range of $[134° \sim 136°] \times [34° \sim 36°]$. Then, the RMSE of the target and ionosphere reflection height is compared under different noise conditions.

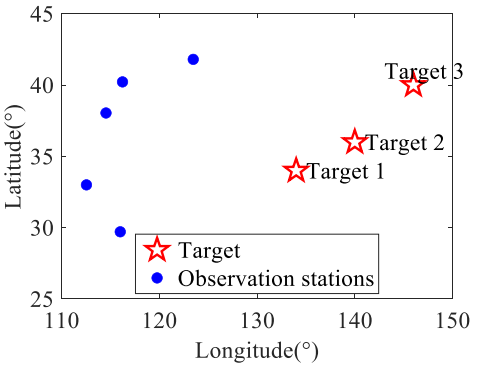

FIGURE 7. Localization geometry.

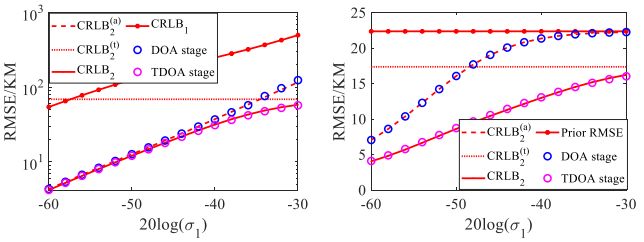

(a) Results of Target 1 (b) Results of ionosphere height

FIGURE 8. Variation of target and ionosphere reflection height accuracy with σ_1 under Target 1.

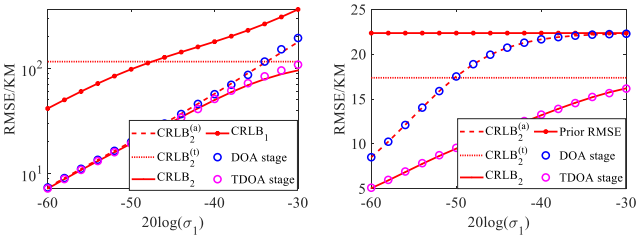

(a) Results of Target 2 (b) Results of ionosphere height

FIGURE 9. Variation of target and ionosphere reflection height accuracy with σ_1 under Target 2.

Parameters of FIGURE 17 are set as $\sigma_{\boldsymbol{\theta}} = 2\sigma_1$(rad), $\sigma_{\boldsymbol{\varphi}} = 3\sigma_1$(rad), $\sigma_{\mathbf{r}} = 1$(KM) and $\sigma_{\mathbf{h}} = 10$(KM). Parameters of FIGURE 18 are set as $\sigma_{\boldsymbol{\theta}} = 0.01$(rad), $\sigma_{\boldsymbol{\varphi}} = 0.015$(rad), $\sigma_{\mathbf{r}} = 10^2\sigma_2$(KM) and $\sigma_{\mathbf{h}} = 2$(KM). Parameters of FIGURE 19 are

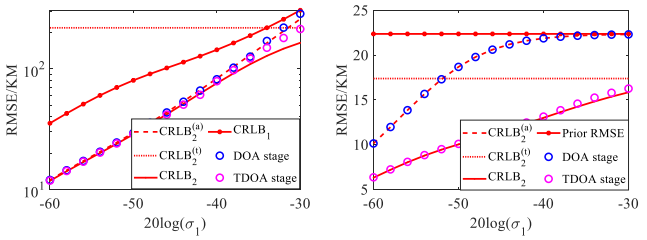

(a) Results of Target 3 (b) Results of ionosphere height

FIGURE 10. Variation of target and ionosphere reflection height accuracy with σ_1 under Target 3.

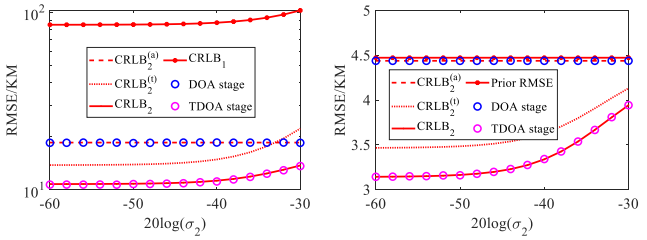

(a) Results of Target 1 (b) Results of ionosphere height

FIGURE 11. Variation of target and ionosphere reflection height accuracy with σ_2 under Target 1.

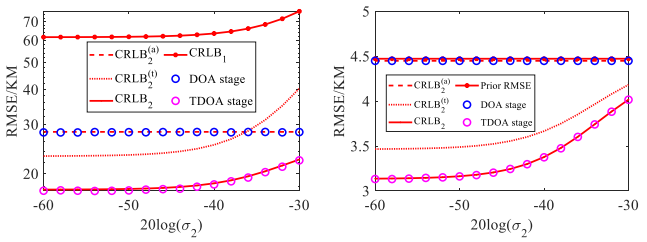

(a) Results of Target 2 (b) Results of ionosphere height

FIGURE 12. Variation of target and ionosphere reflection height accuracy with σ_2 under Target 2.

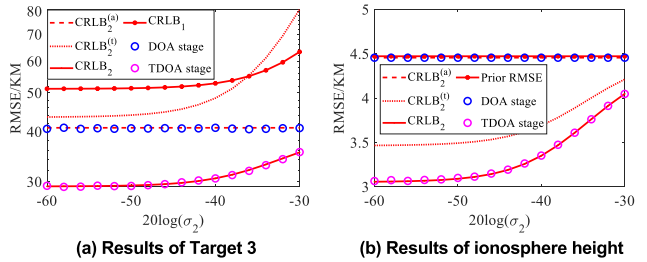

(a) Results of Target 3 (b) Results of ionosphere height

FIGURE 13. Variation of target and ionosphere reflection height accuracy with σ_2 under Target 3.

set as $\sigma_{\boldsymbol{\theta}} = 0.01$(rad), $\sigma_{\boldsymbol{\varphi}} = 0.015$(rad), $\sigma_{\mathbf{r}} = 1$(KM) and $\sigma_{\mathbf{h}} = 5 \times 10^2 \sigma_3$(KM).

From FIGURE 17 to FIGURE 19, the distribution of the estimated results of target and ionosphere reflection height is the same as the corresponding CRLB. The simulation results indicate that the proposed algorithm can reach the CRLB to different target and demonstrate good robustness.

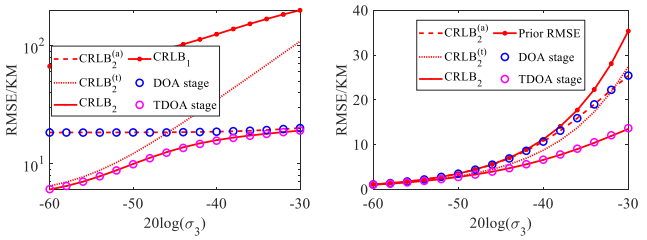

(a) Results of Target 1 (b) Results of ionosphere height

FIGURE 14. Variation of target and ionosphere reflection height accuracy with σ_3 under Target 1.

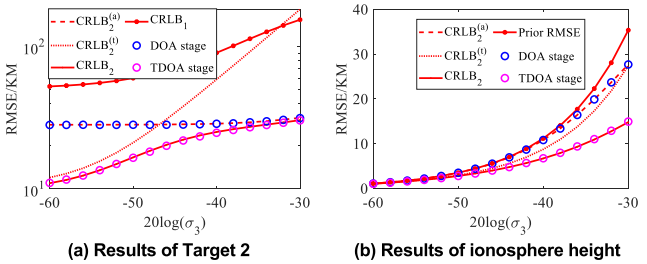

(a) Results of Target 2 (b) Results of ionosphere height

FIGURE 15. Variation of target and ionosphere reflection height accuracy with σ_3 under Target 2.

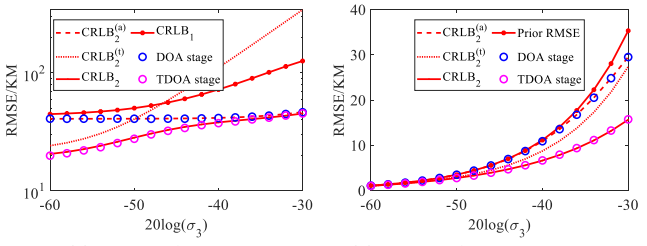

(a) Results of Target 3 (b) Results of ionosphere height

FIGURE 16. Variation of target and ionosphere reflection height accuracy with σ_3 under Target 3.

VII. CONCLUSION

This paper focuses on DOA and TDOA cooperative localization algorithm in short-wave scenario. For the short-wave scenario, this paper proposed a cooperative localization algorithm for joint estimation of target position and ionosphere reflection height using DOA and TDOA measurements. Firstly, based on the IVH model, the DOA and TDOA measurement models are obtained. And the corresponding pseudo-linear equations are established by introducing auxiliary variables. The CRLB is derived for DOA/TDOA hybrid localization, and the target localization accuracy can be effectively improved by introducing the geographic constraint of the target. Then, we proposed to solve the target localization problem combing the differentiable exact penalty method in DOA stage and TDOA stage. In addition, the theoretical analysis of two stages is performed. The theoretical analysis shows that the accuracy of the target and reflection height can reach the corresponding CRLB. Finally, simulations verify that the localization performance of the algorithm can reach the CRLB. Combining the differentiable exact penalty

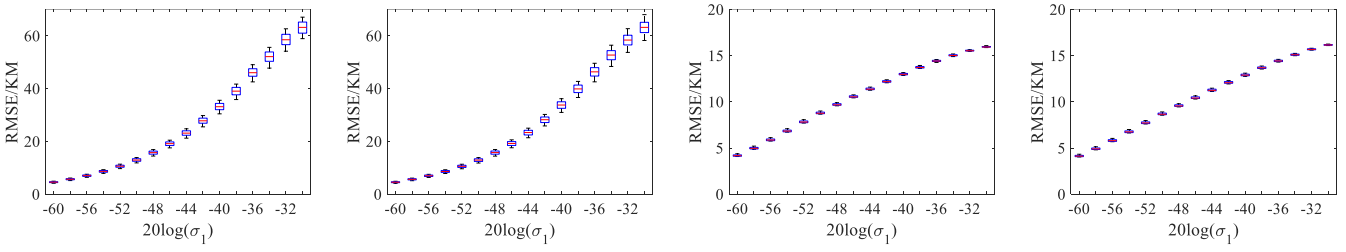

FIGURE 17. Variation of RMSE with σ_1 under different targets.

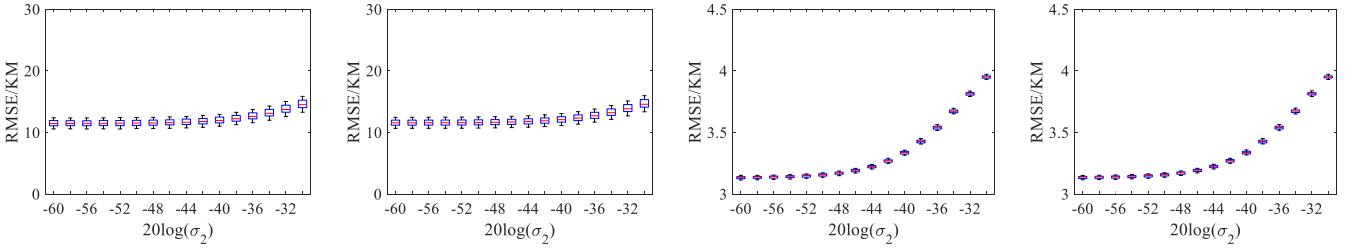

FIGURE 18. Variation of RMSE with σ_2 under different targets.

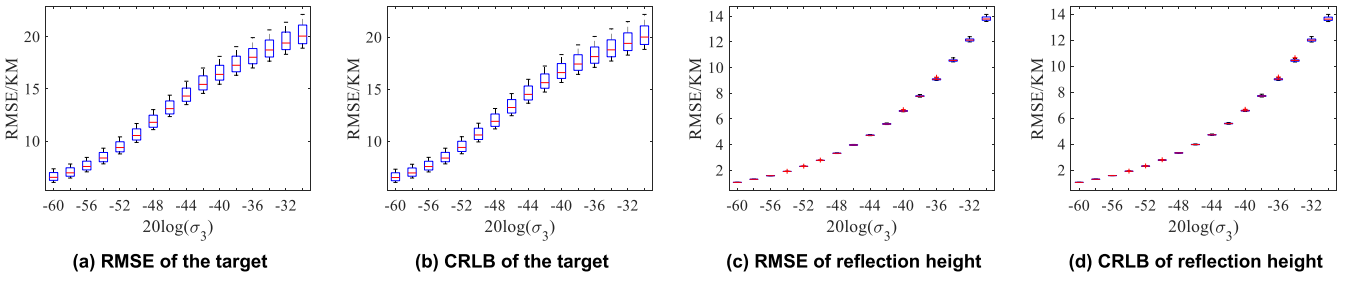

FIGURE 19. Variation of RMSE with σ_3 under different targets.

method can effectively expand the convergence region and reduce the number of iterations. And simulation results also prove that the algorithm is generalizable to the target location.

This paper focuses on short-wave target localization algorithm. In the next step, we will study the use of deep learning to further reduce the influence of ionosphere and thus improve the short-wave localization accuracy.

APPENDIX I

In the practical scenario, we have $R_o > 0$ and $h_i^o > 0$. Furthermore, the range of elevation angle is $0 < \varphi_i^o < \pi/2$, so we have $\cos(\varphi_i^o) > 0$ and $\sin(2\varphi_i^o) > 0$. Based on the definitions of $c_{i,1}$, $c_{i,2}$ and $c_{i,3}$, we can get $c_{i,1} > 0$ $c_{i,2} > 0$ and. $c_{i,3} < 0$. Therefore, we have $(c_{i,2})^2 - 4c_{i,1}c_{i,3} > 0$ which indicates (14) has two roots. And the two roots can be expressed as

$$\begin{aligned} x_1 &= (-c_{i,2} + \sqrt{c_{i,2}^2 - 4c_{i,1}c_{i,3}})/(2c_{i,1}) \\ x_2 &= (-c_{i,2} - \sqrt{c_{i,2}^2 - 4c_{i,1}c_{i,3}})/(2c_{i,1}). \end{aligned} \tag{94}$$

Since $x_1 > 0$ and $x_2 < 0$, x_1 is the only positive root. And (15) is proved.

APPENDIX II

We need to prove

$$\begin{aligned} &\mathbf{CRLB}_1 - \mathbf{CRLB}_1 \times \tilde{\mathbf{\Lambda}}(\tilde{\mathbf{\Lambda}}^{\mathrm{T}}\mathbf{CRLB}_1\tilde{\mathbf{\Lambda}})^{-1}\tilde{\mathbf{\Lambda}}^{\mathrm{T}}\mathbf{CRLB}_1 \\ &\quad = \mathbf{T}_1(\mathbf{T}_1^{\mathrm{T}}(\mathbf{CRLB}_1)^{-1}\mathbf{T}_1)^{-1}\mathbf{T}_1^{\mathrm{T}}. \end{aligned} \tag{95}$$

Based on (31), we can get

$$\mathbf{CRLB}_2 = (\mathbf{CRLB}_1)^{1/2} \times \Pi^{\perp}((\mathbf{CRLB}_1)^{1/2}\tilde{\mathbf{\Lambda}})(\mathbf{CRLB}_1)^{1/2}.$$

Multiplying both sides of (95) by $(\mathbf{CRLB}_1)^{1/2}(\mathbf{CRLB}_1)^{-1/2}$ and then using the definition of the orthogonal projection matrix yields

$$\begin{aligned} &\mathbf{T}_1(\mathbf{T}_1^{\mathrm{T}}(\mathbf{CRLB}_1)^{-1}\mathbf{T}_1)^{-1}\mathbf{T}_1^{\mathrm{T}} \\ &\quad = (\mathbf{CRLB}_1)^{1/2} \times \Pi((\mathbf{CRLB}_1)^{-1/2}\mathbf{T}_1)(\mathbf{CRLB}_1)^{1/2}. \end{aligned} \tag{96}$$

Using the definition of $\mathbf{T}_1$ yields

$$\begin{cases} ((\mathbf{CRLB}_1)^{-1/2}\mathbf{T}_1)^{\mathrm{T}}((\mathbf{CRLB}_1)^{1/2}\tilde{\mathbf{\Lambda}}) = \mathbf{0} \\ rank((\mathbf{CRLB}_1)^{-1/2}\mathbf{T}_1) = 2 + M \end{cases} \tag{97}$$

Furthermore, we can obtain

$$\Pi^{\perp}((\mathbf{CRLB}_1)^{1/2}\tilde{\mathbf{\Lambda}}) = \Pi((\mathbf{CRLB}_1)^{-1/2}\mathbf{T}_1). \tag{98}$$

Substituting (98) into (96) proves that (31) and (32) are equivalent.

APPENDIX III

The following Lagrange function is constructed by Lagrange multipliers.

$$\begin{aligned} &\tilde{\mathrm{L}}_a(\Delta\tilde{\boldsymbol{\eta}}_a, \boldsymbol{\lambda}_a) \\ &\quad = \Delta\tilde{\boldsymbol{\eta}}_a^{\mathrm{T}}\mathbf{\Psi}_a\boldsymbol{\lambda}_a + (\tilde{\mathbf{G}}_a\Delta\tilde{\boldsymbol{\eta}}_a - (\mathbf{C}_1\mathbf{n}_1 + \mathbf{C}_2\mathbf{n}_{\mathbf{h}}))^{\mathrm{T}} \\ &\qquad \times \mathbf{W}_a(\tilde{\mathbf{G}}_a\Delta\tilde{\boldsymbol{\eta}}_a - (\mathbf{C}_1\mathbf{n}_1 + \mathbf{C}_2\mathbf{n}_{\mathbf{h}}). \end{aligned} \tag{99}$$

Making $(\partial\tilde{\mathrm{L}}_a(\Delta\tilde{\boldsymbol{\eta}}_a, \boldsymbol{\lambda}_a)/\partial\Delta\tilde{\boldsymbol{\eta}}_a) = 0$ yields

$$\Delta\tilde{\boldsymbol{\eta}}_a = \mathbf{\Phi}_a\tilde{\mathbf{G}}_a^{\mathrm{T}}\mathbf{W}_a(\mathbf{C}_1\mathbf{n}_1 + \mathbf{C}_2\mathbf{n}_{\mathbf{h}}) - (1/2)\mathbf{\Phi}_a\mathbf{\Psi}_a\boldsymbol{\lambda}_a. \tag{100}$$

Based on $\mathbf{\Psi}_a^{\mathrm{T}}\Delta\tilde{\boldsymbol{\eta}}_a = \mathbf{0}_{2\times 1}$ we have

$$\boldsymbol{\lambda}_a = 2(\mathbf{\Psi}_a^{\mathrm{T}}\mathbf{\Phi}_a\mathbf{\Psi}_a)^{-1}\mathbf{\Psi}_a^{\mathrm{T}}\mathbf{\Phi}_a\tilde{\mathbf{G}}_a^{\mathrm{T}}\mathbf{W}_a(\mathbf{C}_1\mathbf{n}_1 + \mathbf{C}_2\mathbf{n}_{\mathbf{h}}). \tag{101}$$

Substituting (101) into (100) proves (54).

REFERENCES

[1] A. Jain, P. Pagani, R. Fleury, M. M. Ney, and P. Pajusco, "HF source geolocation using an operational TDoA receiver network: Experimental results," *IEEE Antennas Wireless Propag. Lett.*, vol. 17, no. 9, pp. 1643–1647, Sep. 2018.

[2] A. Jain, P. Pagani, R. Fleury, M. M. Ney, and P. Pajusco, "Efficient time domain HF geolocation using multiple distributed receivers," in *Proc. 11th Eur. Conf. Antennas Propag. (EUCAP)*, Mar. 2017, pp. 1852–1856.

[3] T. Wang, X. Hong, W. Liu, A. M. So, and K. Yang, "Geolocation of unknown emitters using TDOA of path rays through the ionosphere by multiple coordinated distant receivers," in *Proc. IEEE Int. Conf. Acoust., Speech Signal Process. (ICASSP)*, Apr. 2018, pp. 3509–3513.

[4] X. Yang and Y. Ye, "Geometric dilution of precision for far-distance TDOA location of shortwave," in *Proc. 2nd Inf. Commun. Technol. Conf. (ICTC)*, May 2021, pp. 60–64.

[5] D. Bilitza, D. Altadill, Y. Zhang, C. Mertens, V. Truhlik, P. Richards, L.-A. McKinnell, and B. Reinisch, "The international reference ionosphere 2012—A model of international collaboration," *J. Space Weather Space Climate*, vol. 4, p. A7, 2014.

[6] D. Bilitza, "The international reference ionosphere—Status 2013," *Adv. Space Res.*, vol. 55, no. 8, pp. 1914–1927, Apr. 2015.

[7] X. Chen, G. Wang, and K. C. Ho, "Semidefinite relaxation method for unified near-field and far-field localization by AOA," *Signal Process.*, vol. 181, Apr. 2021, Art. no. 107916.

[8] N. H. Nguyen and K. Doğançay, "Closed-form algebraic solutions for angle-of-arrival source localization with Bayesian priors," *IEEE Trans. Wireless Commun.*, vol. 18, no. 8, pp. 3827–3842, Aug. 2019.

[9] L. Badriasl and K. Dogancay, "Three-dimensional target motion analysis using azimuth/elevation angles," *IEEE Trans. Aerosp. Electron. Syst.*, vol. 50, no. 4, pp. 3178–3194, Oct. 2014.

[10] F. Pang, K. Doğançay, N. H. Nguyen, and Q. Zhang, "AOA pseudolinear target motion analysis in the presence of sensor location errors," *IEEE Trans. Signal Process.*, vol. 68, pp. 3385–3399, 2020.

[11] R. J. Norman, P. L. Dyson, and J. A. Bennett, "Analytic ray parameters for the quasi-cubic segment model of the ionosphere," *Radio Sci.*, vol. 32, no. 2, pp. 567–577, Mar. 1997.

[12] T. A. Croft and H. Hoogasian, "Exact ray calculations in a quasi-parabolic ionosphere with no magnetic field," *Radio Sci.*, vol. 3, no. 1, pp. 69–74, Jan. 1968.

[13] S. Huang, Y. Pun, A. M. So, and K. Yang, "A provably convergent projected gradient-type algorithm for TDOA-based geolocation under the quasi-parabolic ionosphere model," *IEEE Signal Process. Lett.*, vol. 27, pp. 1335–1339, 2020.

[14] G. Fabrizio and A. Heitmann, "A multipath-driven approach to HF geolocation," *Signal Process.*, vol. 93, no. 12, pp. 3487–3503, Dec. 2013.

[15] G. Wang, X. Jiang, S. G. Razul, C. M. See, and Z. Lin, "Passive TDOA and DOA based HF geolocation without ionosphere information," in *Proc. 10th Int. Conf. Inf., Commun. Signal Process. (ICICS)*, Dec. 2015, pp. 1–5.

[16] T. Zhang, X. Mao, C. Zhao, and J. Liu, "A novel grid selection method for sky-wave time difference of arrival localisation," *IET Radar, Sonar Navigat.*, vol. 13, no. 4, pp. 538–549, Apr. 2019.

[17] W. Ding, J. Yin, and Z. Zhu, "Novel cooperative localization method of over-the-horizon shortwave emitters based on direction-of-arrival and time-difference-of-arrival measurements," *Scientia Sinica Informationis*, vol. 52, no. 11, p. 1942, Nov. 2022.

[18] M. Zhao and Q. Yang, "A new way of estimating ionospheric virtual height based on island multipath echoes in HFSWR," in *Proc. IEEE Radar Conf. (RadarConf)*, Seattle, WA, USA, May 2017, pp. 576–580.

[19] P. Zhu, Y. Zhang, G. Yang, C. Zhou, C. Jiang, and X. Cui, "Development of backscatter sounding single-site location system," *IET Radar, Sonar Navigat.*, vol. 10, no. 3, pp. 632–636, Mar. 2016.

[20] R. J. Norman and P. L. Dyson, "HF radar backscatter inversion technique," *Radio Sci.*, vol. 41, no. 4, pp. 1–10, Aug. 2006.

[21] D. Wang, J. Yin, T. Tang, R. Liu, and Z. Wu, "A two-step weighted least-squares method for joint estimation of source and sensor locations: A general framework," *Chin. J. Aeronaut.*, vol. 32, no. 2, pp. 417–443, Feb. 2019.

[22] M. Sun and K. C. Ho, "An asymptotically efficient estimator for TDOA and FDOA positioning of multiple disjoint sources in the presence of sensor location uncertainties," *IEEE Trans. Signal Process.*, vol. 59, no. 7, pp. 3434–3440, Jul. 2011.

[23] X. Qu, L. Xie, and W. Tan, "Iterative constrained weighted least squares source localization using TDOA and FDOA measurements," *IEEE Trans. Signal Process.*, vol. 65, no. 15, pp. 3990–4003, Aug. 2017.

[24] X. Qu and L. Xie, "An efficient convex constrained weighted least squares source localization algorithm based on TDOA measurements," *Signal Process.*, vol. 119, pp. 142–152, Feb. 2016.

[25] F. Guo and K. C. Ho, "A quadratic constraint solution method for TDOA and FDOA localization," in *Proc. IEEE Int. Conf. Acoust., Speech Signal Process.*, May 2011, pp. 2588–2591.

[26] D. Wang, J. Yin, T. Tang, X. Chen, and Z. Wu, "Quadratic constrained weighted least-squares method for TDOA source localization in the presence of clock synchronization bias: Analysis and solution," *Digit. Signal Process.*, vol. 82, pp. 237–257, Nov. 2018.

[27] Y. Jiexin, W. Ding, Y. Xin, and W. Peng, "Combination of land-based and satellite-based OTH geolocations using differentiable exact penalty method," *IEEE Trans. Aerosp. Electron. Syst.*, vol. 58, no. 3, pp. 2363–2382, Jun. 2022.

[28] V. Karl, I. Neitzel, and D. Wachsmuth, "A Lagrange multiplier method for semilinear elliptic state constrained optimal control problems," *Comput. Optim. Appl.*, vol. 77, pp. 1–39, Sep. 2020.

[29] T. J. Moore, B. M. Sadler, and R. J. Kozick, "Maximum-likelihood estimation, the Cramér–Rao bound, and the method of scoring with parameter constraints," *IEEE Trans. Signal Process.*, vol. 56, no. 3, pp. 895–908, Mar. 2008.

[30] G. H. Golub and C. F. Van Loan, *Matrix Computation*, 4th ed. Baltimore, MD, USA: Johns Hopkins Univ. Press, 2013.

[31] D. P. Bertsekas, *Constrained Optimization and Lagrange Multiplier Methods*. New York, NY, USA: Academic, 1982.

[32] Y. T. Chan and K. C. Ho, "A simple and efficient estimator for hyperbolic location," *IEEE Trans. Signal Process.*, vol. 42, no. 8, pp. 1905–1915, Aug. 1994.

[33] M. Viberg, B. Ottersten, and T. Kailath, "Detection and estimation in sensor arrays using weighted subspace fitting," *IEEE Trans. Signal Process.*, vol. 39, no. 11, pp. 2436–2449, Nov. 1991.

[34] Z. Xianda, *Modern Signal Processing*, 3rd ed. Beijing, China: Tsinghua Univ. Press, 2002.

LINQIANG JIANG received the B.S. degree from PLA Strategy Support Force Information Engineering University, Zhengzhou, China, in 2021, where he is currently pursuing the M.S. degree. His research interests include array signal processing and passive location.

TAO TANG received the degree from the Department of Communication Engineering, Zhengzhou Institute of Information Science and Technology, China, in 2003, and the M.S. and Ph.D. degrees in communication and system engineering from the Zhengzhou Institute of Information Science and Technology, in 2006 and 2011, respectively. From 2012 to 2015, he was an Assistant Professor with the National Digital Switching System Engineering and Technological Research Center (NDSC) and the Zhengzhou Institute of Information Science and Technology. He is currently a Professor in the PLA Strategic Support Force Information Engineering University. His research interest includes array signal processing.

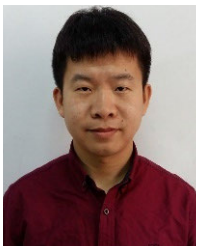

ZHIDONG WU received the B.E. and Ph.D. degrees from the Naval University of Engineering, China, in 2010 and 2013, respectively. He is currently a Lecturer with the National Digital Switching System Engineering and Technological Research Center (NDSC) and PLA Strategic Support Force Information Engineering University. His main research interests include over-the-horizon radar and passive radar.

PAIHANG ZHAO received the B.E. and Ph.D. degrees from the Army Engineering University of PLA, China, in 2015 and 2019, respectively. He is currently a Lecturer with the National Digital Switching System Engineering and Technological Research Center (NDSC) and PLA Strategic Support Force Information Engineering University. His research interest includes array signal processing.

ZIQIANG ZHANG received the B.Sc. degree from PLA Strategy Support Force Information Engineering University, Zhengzhou, China, in 2021, where he is currently pursuing the M.S. degree. His research interests include radiation source localization and signal analysis.